A novel technique for the humidity dependent calibration of hypoiodous acid (HOI) and iodine (I_2)

Lewis Marden[1], Marvin D. Shaw[1], Stephen J. Andrews[1], Maya Zmajkovic[1], Phil Rund[2], Becky Alexander[2], Joel Thornton[2], Andrew Peters[3], Peter Karadakov[4], Lucy J. Carpenter[1]

[1]Wolfson Atmospheric Chemistry Laboratories, Department of Chemistry, University of York, Heslington, York, YO10 5DD, UK
[2]Department of Atmospheric and Climate Sciences, University of Washington
[3]Bermuda Institute of Ocean Sciences, St George's, Bermuda
[4]Department of Chemistry, University of York, Heslington, York, YO10 5DD

Correspondence to: Lewis Marden (lewis.marden@york.ac.uk), Lucy Carpenter (lucy.carpenter@york.ac.uk), Marvin Shaw (marvin.shaw@york.ac.uk)

Abstract. Hypoiodous acid (HOI) and molecular iodine (I_2) are important precursors of reactive gaseous iodine, which plays an important role in the oxidative capacity of the atmosphere and in aerosol formation in the marine boundary layer. HOI and I_2 are emitted from the ocean surface and recycled on atmospheric aerosol via heterogeneous chemistry. Measurements of these molecules, which are typically present in the marine boundary layer at the low-to-sub part per trillion (ppt) level, are sparse, in part due to difficulties in quantification with a lack of appropriate instrumentation and calibration techniques. A novel calibration technique is developed for HOI via generation from I_2 hydrolysis and then 1:1 conversion of HOI back to I_2 through a NaI trap, allowing the sensitivity of HOI to be calculated relative to I_2, which is readily calibrated using a permeation tube system. Using this calibration method, we describe the use of a reduced pressure high resolution chemical ionisation mass spectrometer (CIMS) to characterise the sensitivities of HOI and I_2 over a range of humidities representative of the marine boundary layer and to measure these molecules in the field. At humidities of over 50% RH, the CIMS sensitivity of I_2 is humidity independent whereas HOI exhibits a slight negative humidity dependence. The effect of inlet interactions on HOI and I_2 signals is investigated, with HOI observed to convert to I_2. The implications of these inlet interactions and humidity sensitivities for future ambient measurement configurations are discussed.

1 Introduction

Iodine species play an important role in atmospheric chemistry and climate. They influence the oxidative capacity of the atmosphere through the destruction of ozone (O_3) (Chameides and Davis, 1980; Solomon et al., 1994; Read et al., 2008; Saiz-Lopez et al., 2014; Sherwen et al., 2016a) and alteration of hydrogen oxides (HO_x) and nitrogen oxides (NO_x) cycles (Simpson

et al., 2015; Saiz-Lopez and Von Glasow, 2012). They can also oxidize elemental mercury (Calvert and Lindberg, 2004; Auzmendi-Murua et al., 2014; Lee et al., 2024) and are involved in new particle formation, with iodine oxide radicals (IO), produced during the reaction between O_3 and iodine, self-reacting and further ozonising to form I_2O_5 which can hydrolyse to form HIO_3 (O'dowd et al., 2002; Sipilä et al., 2016; Finkenzeller et al., 2023).

Of the halogens, iodine has the most profound impact on tropospheric O_3 cycling and significantly modifies the atmospheric response to anthropogenic perturbations of ozone precursor emissions. Global model simulations show that atmospheric iodine chemistry lowers the global tropospheric O_3 burden by 6–20% and reduces O_3 concentrations by several parts per billion (ppb), with significant effects over polluted and populated regions (Saiz-Lopez et al., 2014; Sherwen et al., 2016a; Sherwen et al., 2016b; Wang et al., 2021b; Pound et al., 2023; Caram et al., 2023). The dominant source of atmospheric iodine is from the oceans, primarily from the reaction of O_3 and iodide on the sea surface (Garland et al., 1980; Carpenter et al., 2013; Macdonald et al., 2014), resulting in the emission of molecular iodine (I_2) and hypoiodous acid (HOI). HOI is thought to be the largest source, representing ≈75% of iodine emissions into the troposphere (Sherwen et al., 2016a). In the atmosphere, I_2 and HOI rapidly photolyse, producing reactive iodine radicals that catalytically destroy O_3 (Saiz-Lopez and Von Glasow, 2012; Simpson et al., 2015). This cycle represents a negative feedback mechanism, whereby increased O_3 concentrations are offset by increased iodine emissions (Carpenter et al., 2013; Prados-Roman et al., 2015). In fact, model calculations project that future increases in anthropogenic O_3 will be buffered by iodine (Iglesias-Suarez et al., 2020), which has implications for future air quality. Ice core records have shown that there has been a tripling of atmospheric iodine since 1950 (Cuevas et al., 2018; Legrand et al., 2018), likely due to increased anthropogenic O_3 production. Recent measurements of iodine radicals in the lower stratosphere (Koenig et al., 2020) have also demonstrated the potential for iodine to contribute to stratospheric ozone depletion. Iodine has a far higher O_3 destruction potential than chlorine (Klobas et al., 2021) and has been implicated as a potential reason for the unexplained decrease in extra-polar lower stratospheric O_3 (Koenig et al., 2020), which is a region where O_3 changes exert strong radiative effects on climate (Neale et al., 2025).

Despite the significance of HOI and I_2 as the main emission source of atmospheric iodine, and of HOI as a sink for the iodine oxide (IO) radical, there have been few measurements of these compounds. Measurements of I_2, which has been detected by both Differential Optical Absorption Spectroscopy (DOAS) and by Chemical Ionisation Mass Spectrometry (CIMS), have typically been restricted to coastal areas (Saiz-Lopez and Plane, 2004; Bitter et al., 2005; Peters et al., 2005; Mahajan et al., 2009; Huang et al., 2010) with only one measurement in the remote ocean region (Lawler et al., 2014). There has so far been only one directly quantified measurement of HOI, by CIMS, also in a coastal region rather than the open ocean (Tham et al., 2021). There are several challenges that contribute to the scarcity of measurements of these molecules. The mixing ratios of iodine compounds are low, in the sub-ppt to 10 ppt range over the ocean, due to their short atmospheric lifetimes(Saiz-Lopez et al., 2012; Lawler et al., 2014). In addition, halogen compounds can undergo heterogeneous chemistry on the surfaces of instrument inlets, resulting in loss or potentially addition of signal (Neuman et al., 2010; Liao et al., 2012; Liao et al., 2014;

Le Breton et al., 2017; Peng et al., 2022). Further, there is a lack of highly sensitive and selective measurement techniques and instrumentation to measure and quantify these compounds. Given that reactive halogen chemistry is increasingly being incorporated into global chemistry transport models, there is an urgent requirement for observations to help provide constraints and improve model capabilities.

Chemical ionisation mass spectrometry is increasingly being used in the measurement of trace atmospheric gases due to its high sensitivity and selectivity, high time-resolution, soft ionisation, and ability to directly measure compounds in the field with minimal sample preparation (Huey, 2007; Lee et al., 2014; Zhang et al., 2023; Riva et al., 2024). Reagent ions are generated and interact with sample molecules in an ion molecule reactor (IMR) to produce analyte ions, such as through charge transfer or adduct formation reactions. Various reagent ions have been used to measure atmospheric halogen species such as SF_5^- to measure HCl and $ClONO_2$ (Marcy et al., 2005), NO_3^- to measure HIO_3 (Sipilä et al., 2016; Finkenzeller et al., 2023), and SF_6^- to measure bromine and chlorine compounds such as Br_2, Cl_2, BrCl, IBr, and BrO (Sjostedt and Abbatt, 2008; Buys et al., 2013; Roscoe et al., 2014). More recently, I^- has been used for a wide range of chlorine and bromine atmospheric species including Cl_2, Br_2, $ClNO_2$, $BrNO_2$, $ClONO_2$, ClO, BrO, HCl, HOCl, HOBr, BrCl, and various chlorine-containing OVOCs (Kercher et al., 2009; Lee et al., 2014; Custard et al., 2016; Le Breton et al., 2017; Lee et al., 2018; Priestley et al., 2018). However, the I^- reagent ion is not effective in measuring trace levels of iodine species as they can be formed during the generation of the reagent gas (Wang et al., 2021a). An alternative is to use Br^- as a reagent ion. This has previously been used to measure Cl_2, HO_2, H_2SO_4 and HNO_3 (Lawler et al., 2011; Sanchez et al., 2016; Rissanen et al., 2019; Wang et al., 2020) and more recently to detect various iodine species such as I_2, HOI, ICl and IBr using a chemical ionisation atmospheric pressure interface time-of-flight (CI-APi-TOF) mass spectrometer (Tham et al., 2021; Wang et al., 2021a; He et al., 2023). A reduced pressure Br-CIMS has also been developed which can produce analyte ions through an AIM (adduct ionisation mechanism) IMR (Riva et al., 2024). The instrument operates at medium pressures (50–500 mbar) producing low electric fields ($E/N < 10$ Td or field-free conditions), which reduces the chances of fragmentation and promotes adduct formation as the primary method of analyte formation. This loses some of the sensitivity compared to higher pressure CIMS instruments due to the reduced numbers of collisions occurring in the IMR. However, this is compensated for with an increased linear range of detected compounds through promotion of adduct formation.

It has previously been shown that water can form an adduct with halide (I^-, Br^-) reagent ions (R1), which can subsequently act as a reagent ion itself (R3) (Lee et al., 2014; Wang et al., 2021a). The formation enthalpy between a sample molecule and the hydrated reagent ion is lower than with the dry reagent ion (He et al., 2023), and so increasing humidity should result in a decrease in sensitivity, as the proportion of dry reagent ions decreases. However, for small molecules (<8 atoms), increasing humidity has generally been shown to increase sensitivity (Lee et al., 2014; Iyer et al., 2016). This was explained by Quantum Rice-Ramsperger-Kassel (QRRK) theory (Rice and Ramsperger, 1927; Kassel, 1928) which treats the halide adduct cluster as a collection of identical harmonic oscillators (vibrational modes) at ~~an identical~~the same frequency. On formation of the cluster,

the energy produced is distributed amongst the cluster vibrational modes. Not all vibrational modes are considered accessible with experimental evidence suggesting the number of accessible vibrational modes is about half of the total number of vibrational modes (Laidler, 1987). The cluster will fragment if energy above a critical threshold is localised in a single ~~oscillator~~vibrational mode. The rate at which this occurs for a cluster (the decay rate) is calculated by Eq. (1) (Kurtén et al., 2010; Lee et al., 2014).

$$k = \nu \frac{j!(j-m+s-1)!}{(j-m)!(j+s-1)!} \quad (1)$$

where k is the decay rate (s^{-1}), ν is the average vibrational frequency of the cluster (cm^{-1}), s is the number of accessible vibrational modes, m is the quantised binding energy and j is the quantised total thermal energy of the cluster (binding energy plus thermal energy of the individual molecules). m and j are quantised by dividing their calculated energies (cm^{-1}) by ν.

Adding a water molecule to the cluster increases the number of ~~harmonic oscillators~~vibrational modes, which decreases the probability that the critical energy threshold is reached in a single oscillator (Kurtén et al., 2010)~~(KurténN et al., 2010)~~, resulting in a decrease in the ~~rate of fragmentation~~decay rate of the newly formed clusters (R4 and R5). Additionally, a lower energy fragmentation pathway is available for the hydrated adduct (R6), which kicks out the water molecule and keeps the sample molecule and reagent ion together.

$$Br^- + H_2O \rightarrow H_2OBr^- \quad (R1)$$
$$Br^- + A \rightarrow A.Br^- \quad (R2)$$
$$H_2OBr^- + A \rightarrow A.H_2OBr^- \quad (R3)$$
$$A.Br^- \rightarrow Br^- + A \quad (R4)$$
$$A.H_2OBr^- \rightarrow H_2OBr^- + A \quad (R5)$$
$$A.H_2OBr^- \rightarrow A.Br^- + H_2O \quad (R6)$$

where A is the sample molecule.

This kinetic enhancement via the water molecule is in competition with the thermodynamic effect of lower formation enthalpy and will affect different sample molecules to different degrees, requiring the humidity dependence of every molecule of interest to be quantified. Additionally, the humidity dependence will vary between instruments due to differences in IMR conditions and instrument tuning settings.

Formatted: Font: Italic
Formatted: Font: Italic
Formatted: Font: Italic
Formatted: Font: Italic
Formatted: Font: Italic
Formatted: Font: Italic
Formatted: Font: Italic
Formatted: Font: Italic

In this work, the ability for the Br-CIMS to detect and quantify the iodine species I_2 and HOI is demonstrated, and the impact of changing humidity on the instrument sensitivity to these molecules is quantified.

2 Methods

2.1 Bromide Time-of-Flight Chemical Ionisation Mass Spectrometry (CIMS)

The measurement of I_2 and HOI were performed using a Vocus S Chemical Ionisation Time-of-Flight (CI-TOF) Mass Spectrometer (Tofwerk, Switzerland), a high resolution ($R \approx 5000$) instrument that can produce Br^- reagent ions and Br-adduct analyte ions through a Vocus Aim reactor. The operational principles of the instrument and the AIM reactor are described in detail by Riva et al. (2024).

The Br^- reagent ions are generated by passing 0.25 SLPM ultra-high purity N_2 gas over a permeation tube held at 80 °C containing >99% benzene, C_6H_6, and trace amounts of bromoethane, C_2H_5Br. This gas mixture is passed into a vacuum ultraviolet (VUV) ion source where UV light is emitted from a Kr lamp at 116.487 nm and 123.584 nm which is absorbed by the benzene, generating photoelectrons (R7) (Ji et al., 2020; Breitenlechner et al., 2022). These photoelectrons react with the C_2H_5Br, generating Br^- ions (R8) (Riva et al., 2024).

$$C_6H_6 + h\nu \rightarrow C_6H_6^+ + e^- \quad \text{(R7)}$$

$$C_2H_5Br + e^- \rightarrow C_2H_5^\bullet + Br^- \quad \text{(R8)}$$

The Br^- reagent ions are passed into an ion-molecule reactor (IMR) where they are~~it is~~ joined by 1.8 SLPM of sample gas which has been passed into the sampling inlet and through a 0.475 mm critical orifice. The IMR is temperature controlled at 50 °C and pressure controlled at 50 mbar using a vacuum pump (IDP3, Agilent Technologies). The Br^- reacts with sample molecules to form adduct ions. These are drawn through another critical orifice and travel through four differentially pumped chambers which remove neutral molecules and focus the ions into a narrow beam before entering the drift region of the time-of-flight (ToF) chamber. Ions in the TOF chamber are extracted in discrete packets at a frequency of 18.02 kHz and converted into mass spectra using an MCP detector with a preamplifier over a range of 7–510 Th. The extracted packets are averaged over a period of 1 second which is also the speed of data collection. Data averaging, mass calibration, peak assignment, peak fitting and peak integration were all performed using the software package Tofware (version 4.0.1, Aerodyne Research Inc.) used in Igor Pro 9 software (Wavemetrics). This data was then exported and analysed further using the R language for statistical computing (R Core Team).

2.2 Humidity generation

The calibrations performed in this work were made over a humidity range from near complete dryness to almost 100% RH in order to be able to correct for effects caused by variations in ambient humidity in field measurements. This was achieved by humidifying the N_2 gas entering the instrument to various degrees using an in-house dynamic liquid calibration unit (LCU). The operation of this liquid calibration system has been described elsewhere (Yeoman et al., 2022) but is briefly covered here. The LCU is comprised of a proportional liquid-gas mixing valve (Bronkhorst) which controls the mass flow of liquid measured by a mini-Coriolis flow meter (Bronkhorst). It introduces a mass flow controlled zero-air dilution gas to aerosolize and fully evaporate the liquid into a temperature-controlled mixing region. The liquid is pressurized without gas contact, using a custom-built pneumatic cylinder with wetted materials of glass and PTFE.

The gas output of the LCU was maintained at 3.5 SLPM and the water concentration ranged from 0–5 g h^{-1}. During the I_2 calibrations, an additional flow of N_2 gas was used to ~~dilute the humidified flow~~ further increase the gas output. The tubing between the LCU outlet and the additional flow was heated to prevent saturation and condensation of the water vapour.

2.3 Calibration setup

2.3.1 I_2 calibration

An I_2 permeation tube was constructed by adding solid I_2 crystals (99.99%, Sigma-Aldrich) into a ¼" o.d. thin-walled PFA tube with the ends heat sealed closed. The permeation tube was held in a temperature-controlled permeation holder at 40 ~~± 0.1~~ °C. The temperature variation in the holder was minimal, at ± 0.1 °C, and is included in the uncertainty calculation. The permeation tube~~and~~ was continuously swept by 20 sccm high-purity oxygen-free N_2 gas. The emission rate was calculated gravimetrically by measuring the mass ~~loss~~ of the permeation tube over a period of 6 months. Measurements were taken on average every 3 weeks with each data point representing the average of 6 sequential mass measurements, as shown in Fig. A1. ~~several months and~~ The emission rate was calculated from the gradient of Fig. A1 and correspond~~sed~~ to an emission rate of 34.7 ± 0.21 ng min^{-1}~~.~~ with little variation seen during the measurement period.

A schematic of the I_2 calibration setup is shown in Fig. 1. Humidified N_2 gas from the LCU was used to dilute the permeation gas flow~~.~~ and the ~~The~~ CIMS internal sample pump was used to sample thi~~s~~e diluted I_2 permeation gas. Before mixing with the permeation gas, the dilution gas was first split, with some diluting the I_2 permeation gas and some passing through an overflow port. The amount of dilution gas mixing with the permeation gas depends on how much flow the CIMS sample pump pulls towards the instrument. By changing this sample flow rate and hence the dilution of the permeation gas, the concentration of I_2 was altered, allowing for the construction of calibration curves ~~The quantity of dilution flow used for the calibrations was varied by altering the speed of the sample pump, with excess dilution gas from the LCU flowed through an overflow port. Using different pump speeds altered the concentration of I_2, allowing for calibration curves to be constructed~~ at different

humidity levels. Concentrations of I_2 ~~used~~ generated during the calibrations ranged from 1–3 x10^{10} molecules cm^{-3} (600–1000 ppt at SATP).

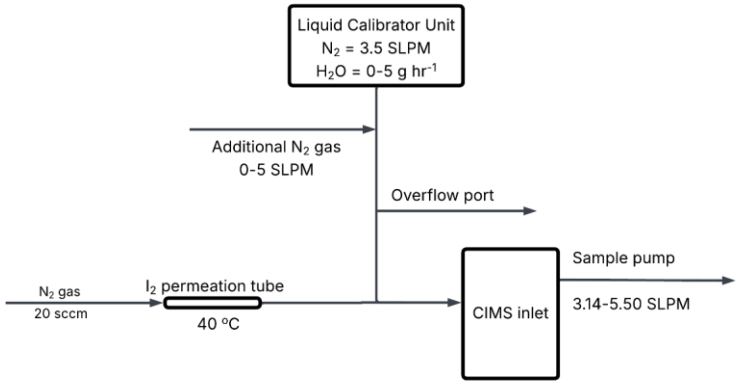

Figure 1: Schematic of the I_2 calibration setup.

2.3.2 HOI calibration

HOI was generated from the hydrolysis of I_2 (R9) in an experimental setup similar to that previously developed for the generation of HOBr in a study by Liao et al. (2012). 500 sccm of N_2 gas was passed over the same I_2 permeation tube from the I_2 calibration and mixed with 500 sccm N_2 gas which had been humidified by passing through a bubbler containing Milli-Q water. This was passed over wetted $AgNO_3$ crystals (99% Fluorochem) in a 9.5 cm long ½" o.d. PFA tube. A small aqueous layer forms on the $AgNO_3$ crystal surface, in which I_2 hydrolysis occurs (R9). The $AgNO_3$ reacts with the generated I^- and H^+ (R-10–12), pushing the (R9) equilibrium in favour of HOI production.

$$I_{2\,(aq)} + H_2O_{(l)} \leftrightarrow HOI_{(aq)} + I^-_{(aq)} + H^+_{(aq)} \quad \text{(R9)}$$

$$AgNO_{3\,(s)} \rightarrow Ag^+_{(aq)} + NO^-_{3\,(aq)} \quad \text{(R10)}$$

$$Ag^+_{(aq)} + I^-_{(aq)} \rightarrow AgI_{(s)} \quad \text{(R11)}$$

$$H^+_{(aq)} + NO^-_{3\,(aq)} \leftrightarrow HNO_{3\,(aq)} \quad \text{(R12)}$$

The resulting I_2 and HOI gas mixture was diluted by humidified N_2 gas from the LCU before being drawn into the CIMS at a flow rate of ≈ 4.1 SLPM. The $AgNO_3$ reactor tube and instrument inlet were wrapped in heating tape and heated to 50 °C to

Formatted: Keep with next

Formatted: Subscript

Formatted: Caption

avoid HOI loss to the tube and inlet walls. The quantification of HOI is achieved by the inclusion of a trap containing sodium iodide (NaI) crystals (99%, Sigma-Aldrich). When the trap is in place, HOI is converted back into I_2 (R13).

$$HOI_{(g)} + NaI_{(s)} \rightarrow I_{2\,(g)} + NaOH_{(aq)} \quad \text{(R13)}$$

The sensitivity of HOI relative to I_2 was found by comparing the HOI signal loss and I_2 signal gain from R13. A 1:1 conversion of HOI to I_2 was assumed, consistent with the approach of Liao et al. (2012) for the equivalent HOBr–Br_2 system. Figure ~~1~~2 shows the simplified schematic of the calibration setup and an idealised example of the relative change between I_2 and HOI. As water is required in the HOI generation step, the calibrations are performed at high humidity. Lowering the humidity of the N_2 gas should allow for lower humidity calibrations, but this will reduce the yield of HOI produced by (R9), making it more difficult to observe the change in I_2 signal.

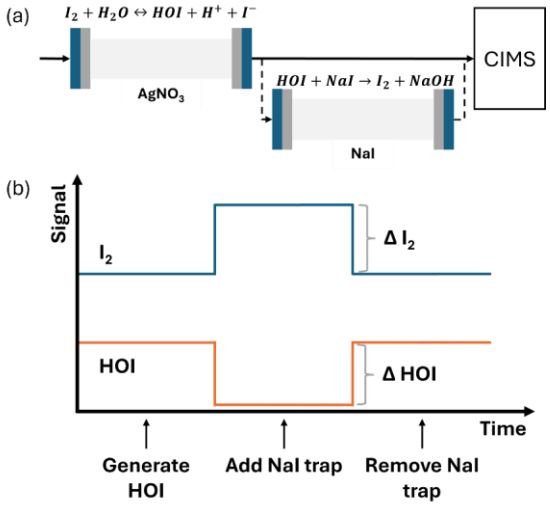

Figure 2~~1~~: (a) A simplified schematic of the HOI calibration setup with reactions shown for HOI generation and destruction. (b) An idealised example of the change in HOI and I_2 signal in the CIMS on addition and removal of the NaI trap.

2.4 Field measurements at Tudor Hill Marine Atmospheric Observatory, Bermuda

The CIMS instrument was deployed during the Bermuda boundary Layer Experiment on the Atmospheric Chemistry of Halogens (BLEACH) field campaign in June 2022. The instrument was stationed at the Tudor Hill Marine Atmospheric Observatory (THMAO) on the west coast of the island of Bermuda (32.26° N, 64.88° W). At this site, the instrument was

placed on top of a temporary sampling tower at 10 metres above ground level and 40 metres above sea level. The ion source gas was supplied by an air compressor connected to a nitrogen membrane and connected to the instrument by ¼" stainless steel tubing. The instrument was contained in an air-conditioned water-resistant enclosure and located at the top of the tower, minimising the potential for inlet effects to occur. The sample inlet was a short (15 cm, ½ in. outer diameter) length of PFA tube. A PTFE guard was placed at the entrance of the inlet tube, with an opening at the bottom, orientated 90° to the inlet. This allowed air to enter at a 90° bend and continue to the instrument while reducing the number of particles entering the CIMS as they impact onto the inlet walls. The sampling rate was 4.1 L min^{-1}, resulting in an inlet residence time of 0.59 s. The Reynolds number was 155, indicating laminar flow once the air was past an 8.5 cm entrance length.

2.5 Quantum chemical calculations

Quantum chemical calculations were used to find the vibrational frequency, binding energy and number of vibrational modes for the adducts $I_2.Br^-$ and $HOI.Br^-$. These were performed using Gaussian 16, Revision C.02 (Frisch et al., 2019), including all electrons in the correlation calculations through "MP2(Full)" and "CCSD(T,Full)". The geometries of the adducts were optimised at the MP2 level and then single-point energies were calculated, at these geometries, at the CCSD(T) level. All geometry optimisations were carried out under the "VeryTight" convergence criteria, and the optimised geometries were confirmed as local minima through subsequent frequency calculations. All calculations used the standard aug-cc-pVTZ basis set for all atoms except iodine, and the aug-cc-pVTZ-PP ECP basis from the Basis Set Exchange (Pritchard et al., 2019) for iodine. We refer to this combination as "aug-cc-pVTZ-PP'". Binding enthalpies were obtained by adding together the energy difference E (complex) – E (reactants) at the CCSD(T) level to the corresponding difference between the thermal corrections to the enthalpy at the MP2 level (the thermal corrections to the enthalpy involve vibrational contributions, hence the need to have these at the level at which the geometries were optimised). The values are shown in Table 1.

Table 1: The calculated vibrational frequencies, binding energy, total thermal energy and vibrational modes of the $I_2.Br^-$ and $HOI.Br^-$ clusters. The decay rate is found using Eq. (1).

Cluster	Vibrational frequency / Hz	Binding energy / kcal mol^{-1}	Total thermal energy / kcal mol^{-1}	Vibrational modes (accessible)	Decay rate / s^{-1}
$I_2.Br^-$	3.06×10^{12}	30.8	33.5	4 (2)	2.66×10^{11}
$HOI.Br^-$	1.19×10^{13}	24.3	27.1	6 (3)	2.38×10^{11}

Formatted: Heading 2
Formatted: Subscript
Formatted: Superscript
Formatted: Caption, Keep with next
Formatted: Superscript
Formatted: Centered
Formatted: Centered
Formatted: Centered
Formatted Table
Formatted: Centered
Formatted: Centered
Formatted: Centered
Formatted: Centered
Formatted: Centered
Formatted: Centered

3. Results and Discussion

3.1 Detection of iodine compounds

I_2 and HOI were detected as adducts with Br^-, with the two $I_2.Br^-$ isotopes observed at m/Q 332.73 and 334.73 Th and the two $HOI.Br^-$ isotopes at 222.83 and 224.83 Th. The single peak mass spectra fits for I_2 are shown in Fig. ~~2~~3, and in Fig. 4 for HOI, taken from an HOI calibration experiment and of ambient air at Tudor Hill, Bermuda. At the instrument resolution of 5000, the high mass defect of the $I_2.Br^-$ adduct allows it to be clearly differentiated from other peaks ~~at 333 m/Q as seen in Fig. 2 d–f,~~ even during ambient conditions at low mixing ratios. The $HOI.Br^-$ adduct has a smaller mass defect, and subsequently has more overlap with interferent peaks. During the HOI generation stage of the calibration (Fig. ~~4~~2a), the HOI signal is significantly greater than any interferent peaks. However, on addition of the NaI trap (Fig. ~~4~~2b), or during ambient measurements (Fig. ~~4~~2~~c~~e), the HOI signal overlaps with other interferent peaks. Despite this, the resolution is sufficient for Tofware's multi-peak fitting algorithm (Stark et al., 2015) to identify HOI even at very low mixing ratios. The signal can be further verified by examining the fit of the HOI isotope peak (Fig 4. d–f), calculated by the Tofware software. Detection limits during field conditions are discussed in Sect.~~section~~ 3.7.

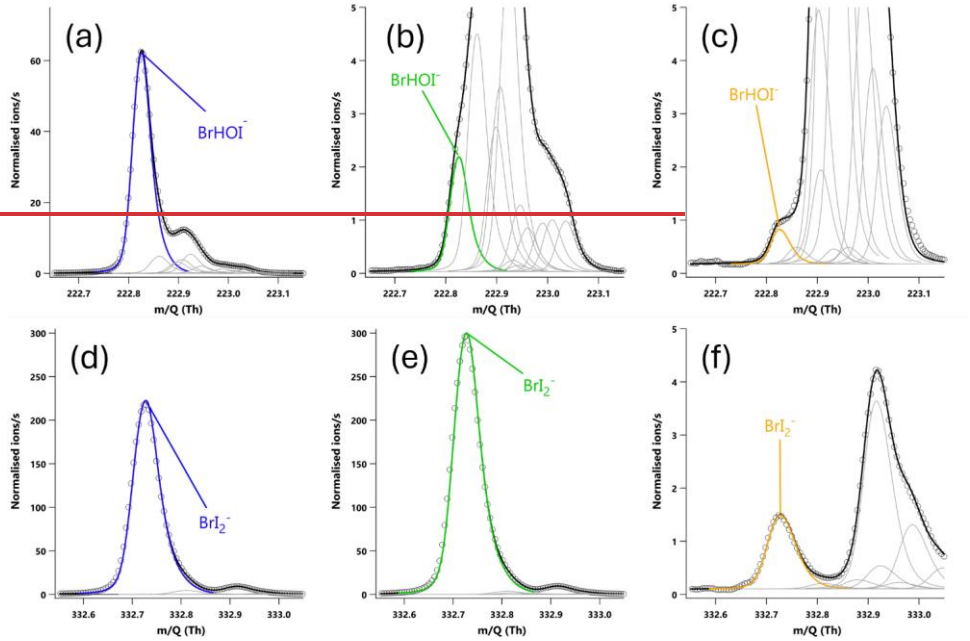

Figure 2: 20-minute averaged high resolution single peak mass spectra fits for HOI (a,b,c) and I_2 (d,e,f). The signal intensities correspond to mixing ratios of (a) 60.8 ppt, (b) 2.2 ppt, (c) 0.87 ppt, (d) 190.2 ppt, (e) 254.0 ppt and (f) 1.37 ppt. (a) The signal of HOI and (d) I_2 during an HOI calibration run without the NaI trap. (b) The signal of HOI and (e) I_2 during an HOI calibration run on addition of the NaI trap. (c) Ambient air measurements of HOI and (f) I_2 in a high humidity environment.

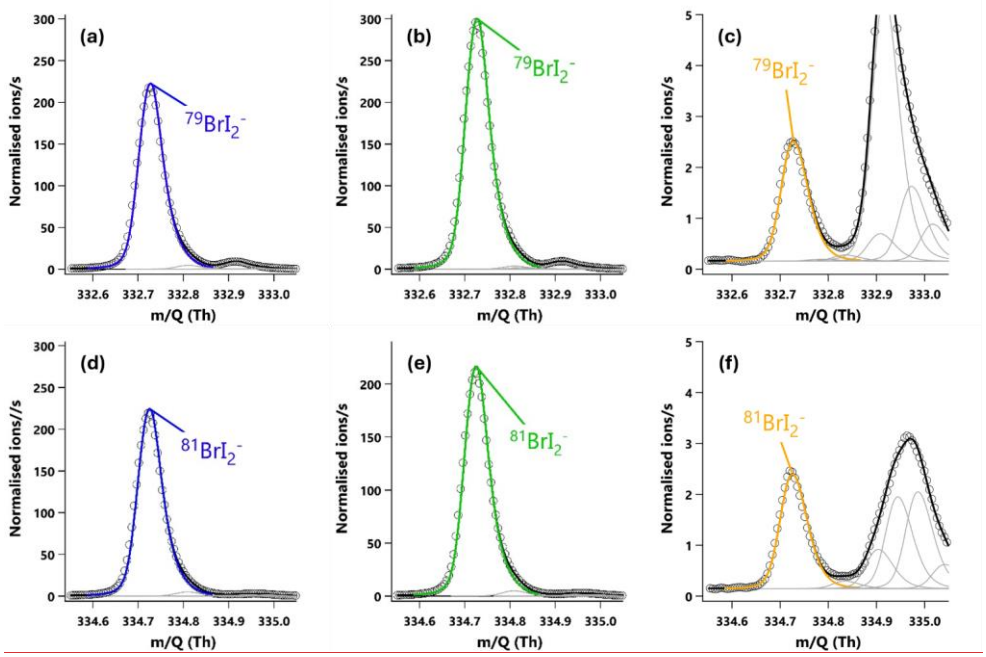

Figure 3: 20-minute averaged high resolution single peak mass spectra fits for the molecular ion peak (a,b,c) and primary isotope peak (d,e,f) for I_2. The signal intensities correspond to mixing ratios of (a) 190.2 ppt, (b) 254.0 ppt and (c) 1.37 ppt. (a, d) The I_2 signal during an HOI calibration run without the NaI trap. (b, e) The I_2 signal during an HOI calibration run on addition of the NaI trap. (c, f) Ambient air measurements of I_2 in a high humidity environment.

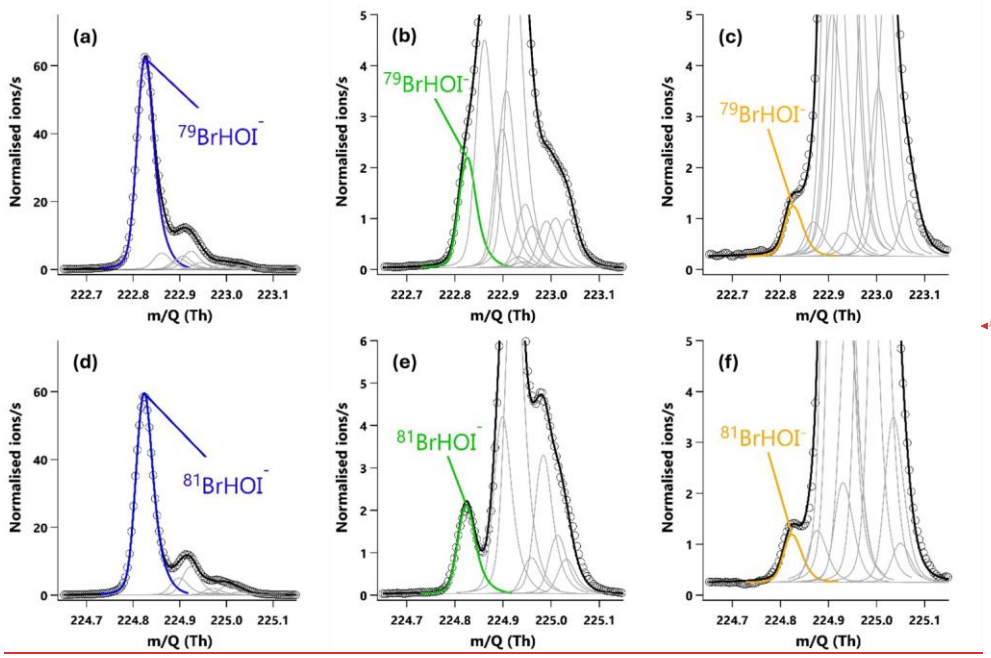

Figure 4: 20-minute averaged high resolution single peak mass spectra fits for the molecular ion peak (a,b,c) and primary isotope peak (d,e,f) for HOI. The signal intensities correspond to mixing ratios of (a) 60.8 ppt, (b) 2.2 ppt and (c) 0.87 ppt. (a, d) The HOI signal during an HOI calibration run without the NaI trap. (b, e) The HOI signal during an HOI calibration run on addition of the NaI trap. (c, f) Ambient air measurements of HOI in a high humidity environment.

3.2 Signal normalisation

The I_2 and HOI adducts are formed from a pseudo first order reaction between the sample molecules and the Br^-/H_2OBr^- reagent ions, and the adduct signal intensity is proportional to the reagent ions available. During experiments, the quantity of available reagent ions fluctuates over time. This can be due to variations in the efficiency of the ion source in generating the reagent ions, or with slight changes within the instrument. This variation can be corrected for by normalising the analyte signal against the sum of the reagent ions measured by the instrument, shown in Eq. (~~1~~2). For CIMS instruments, the normalised signal is typically reported per million reagent ions, with units of normalised counts per second per million reagent ion counts per second (ncps). It has been reported that normalisation can compensate up to 50% reagent ion depletion from sample molecules (Riva et al., 2024).

Formatted: Keep with next

Formatted: Caption, Space After: 0 pt, Border: Top: (No border), Bottom: (No border), Left: (No border), Right: (No border), Between : (No border)

Formatted: Font: Not Bold, Font color: Auto

$$Normalised\ signal\ (ncps) = \frac{A.Br^-\ (cps)}{Br^-\ (cps) + H_2OBr^-\ (cps)} * 10^6 \quad (1)$$

where A is the sample molecule.

3.3 I_2 humidity dependence

The humidity of the instrument IMR, where the reagent ion collisions occur, is not directly measured but has been related to the sample relative humidity (Wang et al., 2021a; He et al., 2023) and/or vapour pressure of water (Lee et al., 2014; Lee et al., 2018). An alternative method is to use the ratio between the first reagent ion water cluster, H_2OBr^-, and the dry reagent ion, Br^- (Dörich et al., 2021)~~(DöRich et al., 2021)~~, Eq. (2). This has the advantage of not requiring further equipment to measure humidity levels during calibrations and accounts for any changes that may occur when the gas flows through the inlet. The so-called "water ratio" is used hereon to represent humidity. The water ratio is compared against absolute humidity measured during the BLEACH campaign in Fig. A4. Previous studies have shown that IMR temperature can impact the proportions of the hydrated and dry reagent ions, though this has been performed over a wide range of temperatures (Robinson et al., 2022). Fig. A4 shows that there was little variation in the IMR temperature (±0.6 °C) and pressure (±0.35 mbar) during the BLEACH campaign and that these changes did not noticeably affect the water ratio at different humidities.

$$water\ ratio = \frac{H_2OBr^-\ (cps)}{Br^-\ (cps)} \quad (2)$$

I_2 calibrations were performed at a range of different humidities generated by changing the water mass supplied by the LCU. The range of I_2 concentrations for each humidity was between 1–3 ~~x~~×10^{10} molecules cm^{-3}; about two orders of magnitude higher than what would typically be observed in the atmosphere. Ideally, the concentration range would be comparable to atmospheric levels, but limitations in the amount of gas dilution and water mass flow restricted the minimum concentrations that could be used. Low pressure CIMS instruments reportedly have large linear ranges, particularly when normalising to the reagent ion (Riva et al., 2024), and so it is assumed in this work that the calibration range is within the linear range of the instrument. The I_2 sensitivity was determined by calculating the gradient of the calibration curves with units of ncps cm^3 $molecules^{-1}$. The instrument response over the calibration range demonstrated a high degree of linearity, an example of which is shown in Fig. ~~3~~5.

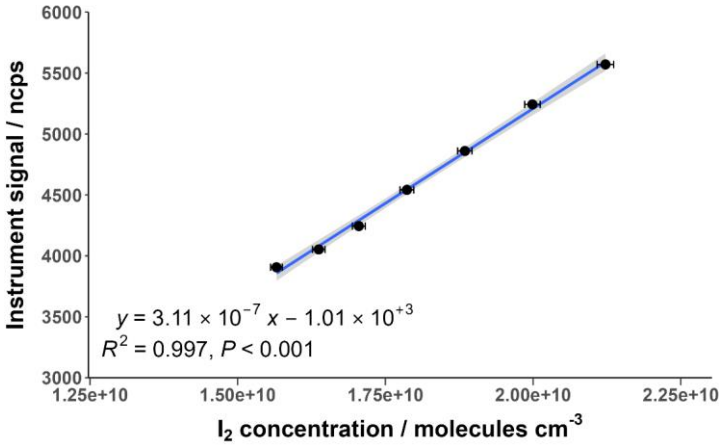

Figure 5: Normalised instrument signal against I_2 concentration for an example calibration at a water ratio of 1.05. The shaded area represents the 95% confidence interval of the fitted curve. Error bars indicate the calculated propagated uncertainty of the I_2 concentration, shown in Sect.~~section~~ 3.5.

The change in I_2 sensitivity at different humidities is demonstrated in Fig 46. Above a water ratio of ~0.7, the sensitivity of I_2 is effectively humidity-independent with a sensitivity of 3.25×10^{-7} ($\pm 6.30 \times 10^{-9}$) ncps cm^3 $molecules^{-1}$. This is four times more sensitive than the average sensitivity of 7.92×10^{-8} ($\pm 3.18 \times 10^{-9}$) ncps cm^3 $molecules^{-1}$ at near dryness (average water ratio = 0.0022), which can be attributed to the stabilising effect of the H_2O molecule on the formed adduct. As humidity is increased,~~At high humidities,~~ this stabilising effect is balanced out by more adduct formation occurring via the ~~the lower formation enthalpy of adducts formed with the~~ BrH_2O^- reagent ion, which is a less exothermic reaction (Wang et al., 2021a). There is also an increase in the formation of the second water cluster, $Br(H_2O)_2^-$, at very high humidities, shown in Fig 7. There appears to be no literature on whether this cluster also acts as a reagent ion for I_2. However, it is unlikely to act as one due to an additional collisional reaction needed for formation of $Br(H_2O)_2^-$ and the likely even lower formation enthalpy between the second water cluster and a sample molecule. The second water cluster may have an indirect effect on the reduction of the increase in sensitivity. At very high humidities, the proportion of dry reagent ion continues to decrease with the first water cluster proportion remaining steady while the second water cluster increases. This suggests the formation rate of the first water cluster is being matched by its conversion to the second water cluster. This will still reduce the amount of adduct formation occurring through the more exothermic dry reagent ion pathway but will not produce an increase in sensitivity via water stabilisation. These factors potentially explain the emergence of the humidity-independent region above the 0.7 water ratio.

Formatted: Caption, Don't keep with next

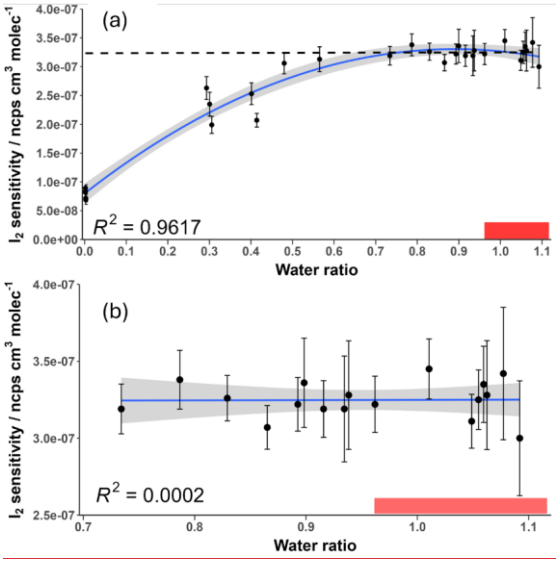

Figure 6: Measured I_2 sensitivity at different humidity levels over (a) the full range and (b) the humidity-independent range. Error bars represent the calculated error for each sensitivity value described in Sect. 3.5. The shaded grey area represents the 95% confidence interval of the fitted curve. The shaded red region represents the ambient water ratio observed in the marine boundary layer at Tudor Hill, Bermuda. The dotted line in (a) is the average of the data points in (b).

Formatted: Caption, Don't keep with next

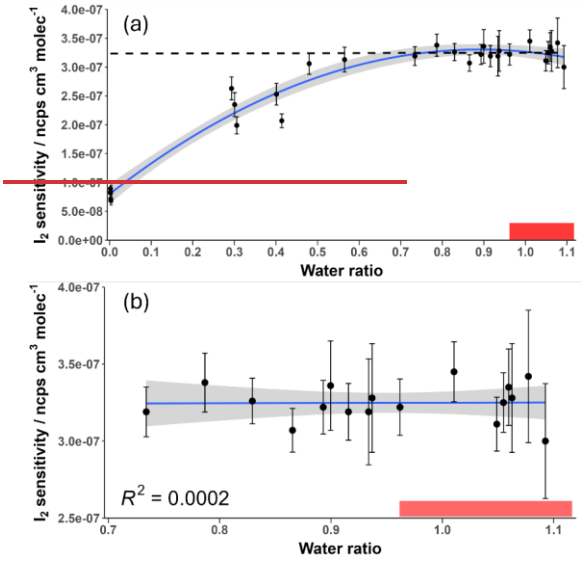

~~**Figure 4: Measured I_2 sensitivity at different humidity levels over (a) the full range and (b) the humidity-independent range. Error bars represent the calculated error for each sensitivity value described in section 3.5. The shaded grey area represents the 95% confidence interval of the fitted curve. The shaded red region represents the ambient water ratio observed in the marine boundary layer at Tudor Hill, Bermuda. The dotted line in (a) is the average of the data points in (b).**~~

Formatted: Keep with next

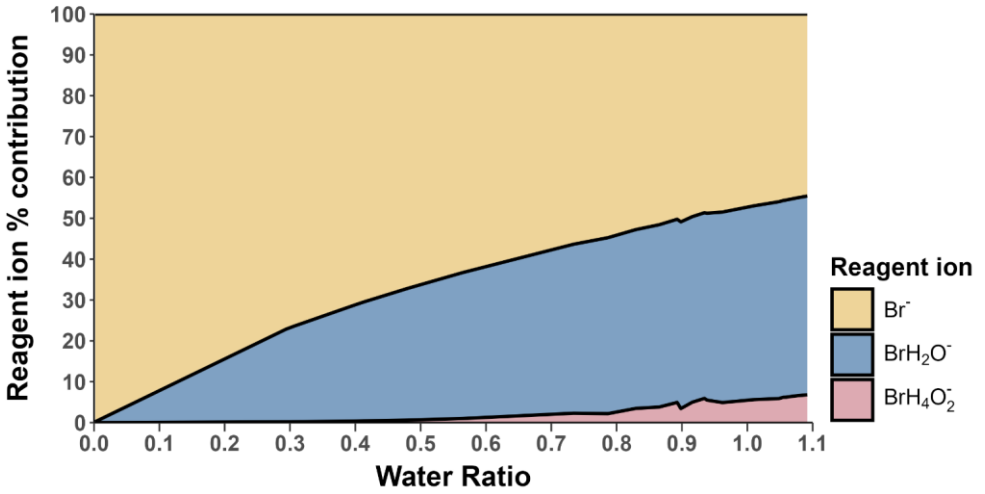

Figure 7: The percentage contribution of the Br^- ion (yellow), BrH_2O^- ion (blue) and $BrH_4O_2^-$ ion (pink) at different water ratios. The values shown are the average contributions of these ions detected during the I_2 calibration runs.

3.4 HOI calibration and humidity dependence

The relative sensitivity of HOI compared to I_2 (termed the HOI/I_2 ratio) was quantified by comparing the change in signal of HOI and I_2 with and without the NaI trap in place, with an example calibration shown in Fig. ~~5~~8. With no trap in place, the ratio of HOI to I_2 signal was found to be around 1:5. On addition of the NaI trap, almost all of the HOI signal was removed with a corresponding increase in I_2 signal observed. For the equivalent HOBr–Br_2 system in the Liao et al. (2012) system, the conversion of HOBr to Br_2 was assumed to be 1:1. Here, the 1:1 HOI to I_2 conversion assumption was tested by measuring the signal of various other iodine-containing compounds, to determine whether any other significant reaction pathways were occurring during the production and destruction of HOI. The mass spectra of these other iodine compounds are shown ~~without~~ including the NaI trap in Fig. A2~~1~~ and ~~including~~ without the trap in Fig. A3~~2~~. Some of these compounds have substantial overlapping interfering peaks, and it is not possible at the instrument resolution to determine how real their signals are. Of these compounds, only HI and IBr had both distinct enough peaks and showed a small increase on~~On~~ addition of the NaI trap.~~,~~ ~~a small increase in signal was observed for HI and IBr.~~ The~~se~~ ~~quantities~~increase in HI and IBr signals were much smaller than for I_2, which represented 96% of the change in signal, as shown in Table A1. The production of HI is likely from the reaction of NaI and HNO_3, which is produced via (R12) in the HOI generation step, rather than from HOI. It is possible that the ~~HI and~~ IBr signal may be produced from HOI, for example if there was some contaminant NaBr also present in the trap.

Formatted: Font color: Auto

Formatted: Caption, Space After: 0 pt, Border: Top: (No border), Bottom: (No border), Left: (No border), Right: (No border), Between : (No border)

Formatted: Subscript

~~However~~Conversely, any contaminant bromine compounds in the gas stream may react with the NaI trap, producing the IBr. However, the average standard error of the I_2 signal change is already higher than the increase in IBr signal, and so the production of IBr can be considered negligible against the other uncertainties of the calibration and the assumed 1:1 conversion of HOI to I_2 can be maintained.~~it is also possible that the presence of NaI is the cause of these compounds, such as any contaminant bromine compounds reacting with NaI to produce IBr. Either way, the intensity of the signals for HI and IBr can be considered negligible and therefore substantiate the assumption of 1:1 conversion of HOI to I_2.~~

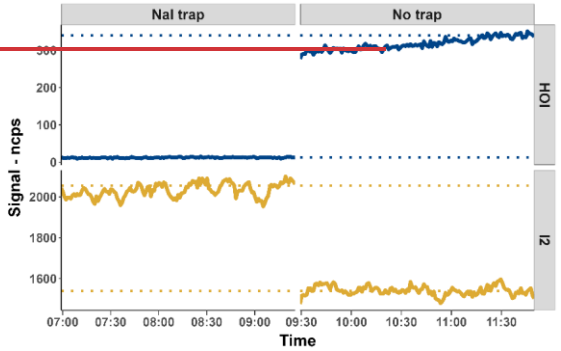

~~**Figure 5: The 1-minute averaged HOI and I_2 normalised signal with and without the inclusion of the NaI trap. Dotted lines indicate the average signal of the final 20 minutes of each run.**~~

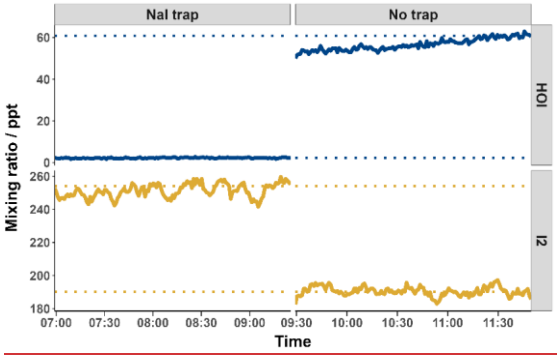

Figure 8: 1-minute averaged HOI and I_2 mixing ratios with and without the inclusion of the NaI trap. Dotted lines indicate the average mixing ratio of the final 20 minutes of each run. Values were calculated according to the calibration curve from Fig 9.

Formatted: Caption, Space After: 0 pt, Border: Top: (No border), Bottom: (No border), Left: (No border), Right: (No border), Between : (No border)

Formatted: Font color: Auto

The HOI calibration experiments were performed at different water ratios to determine how the HOI/I_2 ratio changes with humidity. As water was required to generate HOI in the first stage of the calibration, the experiments were only able to be performed at relatively high humidity, between water ratios of 0.7 and 1.1. This range corresponds to the humidity-independent region found for I_2. The humidity dependence of the HOI/I_2 ratio is shown in Fig. ~~6~~9.

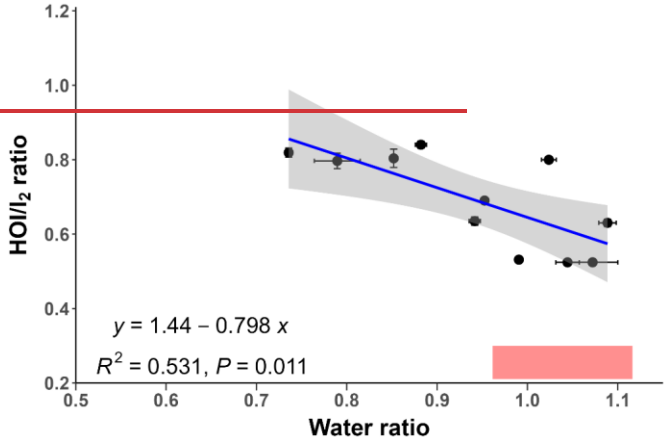

~~**Figure 6: The relative sensitivity of HOI compared to I_2 (HOI/I_2 ratio) at different water ratio values. The shaded grey area represents the 95% confidence interval of the fitted regression line. The shaded red region represents the ambient water ratio observed in the marine boundary layer at Tudor Hill, Bermuda.**~~

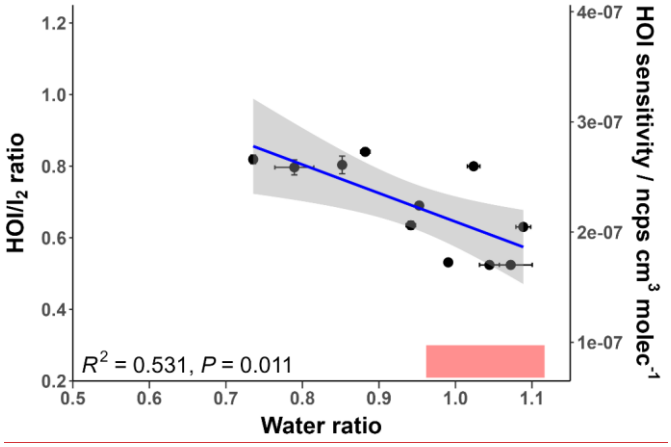

Figure 9: The relative sensitivity of HOI compared to I_2 (HOI/I_2 ratio) at different water ratio values. The regression line follows the equation y = 1.44 - 0.798x. The secondary y-axis shows the corresponding HOI sensitivity compared to the HOI/I_2 ratio. The shaded grey area represents the 95% confidence interval of the fitted regression line. The shaded red region represents the ambient water ratio observed in the marine boundary layer at Tudor Hill, Bermuda.

Formatted: Caption, Don't keep with next

Figure ~~6~~ 9 shows that the HOI/I_2 ratio moderately correlates with increasing humidity; the correlation is statistically significant with a P-value below 0.05. As the humidity dependence of I_2 is independent over this measurement range, this decrease is attributed to a decreasing sensitivity for HOI. This can be explained from a QRRK theory standpoint. As seen in Table 1, ~~T~~the $HOI.Br^-$ cluster has more accessible vibrational modes~~harmonic oscillators~~ than $I_2.Br^-$, so the increase ~~of harmonic oscillators~~in vibrational modes from the presence of water ~~has~~ will have a smaller stabilising effect for $HOI.Br^-$ than for $I_2.Br^-$. Additionally, ~~as~~ the formation enthalpy for the $HOI.Br^-$ cluster is lower than for $I_2.Br^-$ ~~(He et al., 2023)~~, and so the effect of reducing the amount of ~~dry cluster~~ formation via the dry reagent ion has a more pronounced effect on the $HOI.Br^-$ cluster.

3.5 Sensitivity measurement uncertainty

Propagation of error was used to calculate the uncertainty of the I_2 and HOI sensitivities. This can be calculated using the exact formula of propagation, assuming that variables are independent of each other, as shown in Eq. (~~3~~4).

$$\sigma_x = \sqrt{(\frac{\partial_x}{\partial_a})^2.\sigma_a^2 + (\frac{\partial_x}{\partial_b})^2.\sigma_b^2 + (\frac{\partial_x}{\partial_c})^2.\sigma_c^2 + \cdots + (\frac{\partial_x}{\partial_n})^2.\sigma_n^2} \quad (~~3~~4)$$

where a, b, c, …, n are the variables of the function x, ∂_x/∂_n is the partial derivative of the variable with respect to x, and σ_n is the error of the individual variable.

3.5.1 I_2

The I_2 concentration error was calculated from the propagation of the uncertainties of the emission of the I_2 permeation tube, the temperature of the permeation tube holder, and the total gas flow from the sample pump to give a relative error of 0.7%. The uncertainty of the sensitivity from a specific humidity calibration was calculated from the propagated uncertainty of the I_2 concentration and the instrument signal for each point in the calibration curve, as shown in Fig. 5~~3~~. The uncertainties of the sensitivities in the humidity independent region can be averaged using Eq. (45) as these can be considered as repeats.

$$\sigma_{humidity\ independent\ sensitivity} = \frac{\sqrt{\sum_{i=1}^{n}(\sigma_i)^2}}{n} \quad (45)$$

where σ_i is the uncertainty of a particular sensitivity measurement and n is the number of measurements made in the humidity independent region.

This resulted in a sensitivity uncertainty of 6.30×10^{-9} ncps cm^3 molecules^{-1} for the humidity-independent region, corresponding to a relative error of 1.9%. This was repeated for the dry calibration sensitivities to produce an uncertainty of 3.18×10^{-9} ncps cm^3 molecules^{-1} which represents a relative error of 4.0%. This uncertainty encompasses both calibration and humidity-dependence uncertainties, but not background (zero) or inlet effects (see Sect. 3.6).

3.5.2 HOI

The sensitivity of HOI was determined relative to I_2 based on the linear model in Fig. ~~5~~9. The uncertainty of the HOI sensitivity at a specific water ratio was found from the uncertainty of the I_2 sensitivity at that water ratio propagated with the uncertainty of the gradient and intercept of the linear model. This results in an uncertainty of 4.29×10^{-8} ncps cm^3 molecules^{-1} for the HOI sensitivity, corresponding to an average relative error of 19.8% with a range of 16-25%, neglecting any background and inlet effects.

3.6 Inlet loss considerations

Measuring gas-phase compounds through an instrument inlet will introduce gas-wall interactions that can lead to loss of signal or require conditioning to reach a steady state (Krechmer et al., 2016; Huang et al., 2018; Deming et al., 2019). Additionally, halogen compounds can undergo heterogeneous chemistry on inlet walls, resulting in conversion to other halogen compounds. This is particularly the case for the hypohalous acids and has been observed for HOBr and HOCl when measured by CIMS instruments (Neuman et al., 2010; Liao et al., 2014; Le Breton et al., 2017; Peng et al., 2022). While all halogen compounds

experience these wall interactions, it is particularly pronounced for iodine compounds, leading to large losses and uncertainties in measurements. Previous measurements of I_2 have found sample line losses between 18–40% (Shaw and Carpenter, 2013; Carpenter et al., 2013). For HOI, the calibration performed by Tham et al. (2021) modelled the loss of HOI through their inlet system via diffusion to the inlet walls which contributed to their total HOI uncertainty of ± 55%.

The effect of inlet losses is heavily influenced by the instrument setup. This means that any differences in inlet configuration between calibrations and field measurements need to be accounted for. When deployed in the field, the inlet for this instrument had a PTFE guard, allowing sample air to enter the inlet at a 90° angle, shown in Fig. ~~7b~~10b. The guard was implemented with the intention that light gas-phase molecules could navigate around the bend without loss to the walls, but heavier aerosol particles could not, reducing the potential for aerosol to block the entrance to the CIMS instrument. However, when calibrating, the calibration gas was directed linearly into the sampling inlet, shown in Fig. ~~7a~~10a. The effect of this difference was investigated.

Two inlet loss experiments were performed, one using a PFA T-piece to investigate the effect of physically having a bend in place, and another with the PTFE guard that had been salted with sea water to mimic field conditions. A line of 1/8" PFA tubing was attached to the output of the HOI calibration system and held in two configurations: one where it is pushed past the bend as shown in Fig. ~~7c~~ 10c and one where it is held before it, Fig. ~~7d~~10d. This required altering the dilution flow to laboratory air to accommodate this configuration. The effect of the T-piece and PTFE guard on the normalised signal of HOI and I_2, along with other iodine compounds that are potentially present, are shown in Table ~~1~~2.

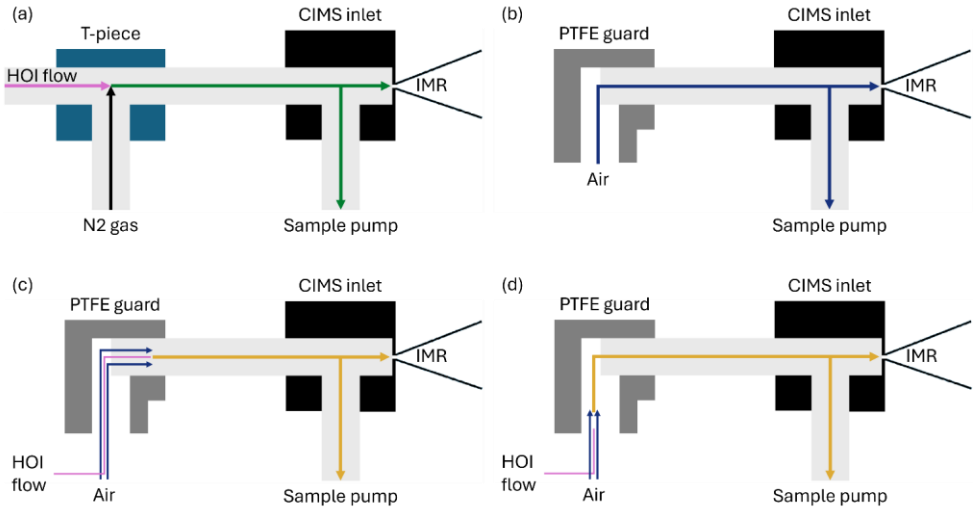

Figure 10: Simplified diagrams of the CIMS inlet setup during (a) the HOI calibration experiments, (b) sampling of air at Tudor Hill in Bermuda, (c) the line loss experiment bypassing the PTFE guard bend, (d) the line loss experiment including the bend from the PTFE guard.

Table 2: The normalised signal ± 1 standard deviation of various iodine species measured during the direct and bended inlet configurations for the T-piece and PTFE guard inlet loss experiments.

Species	T-piece			PTFE guard		
	Direct configuration ± 1σ / ncps	Bend configuration ± 1σ / ncps	Signal difference / ncps (% change)	Direct configuration ± 1σ	Bend configuration ± 1σ	Signal difference / ncps (% change)
HOI	381.45 ± 5.85	132.79 ± 6.38	-248.66 (-65%)	335.05 ± 5.79	85.13 ± 2.59	-249.92 (-75%)
I_2	2576.62 ± 25.92	2985.40 ± 49.75	+408.78 (+16%)	2149.51 ± 23.18	2472.60 ± 25.23	+323.09 (+15%)
ICl	371.44 ± 8.45	375.98 ± 10.53	+4.54 (+1%)	400.73 ± 8.62	531.58 ± 15.02	+130.85 (+33%)
IBr	20.82 ± 1.47	17.34 ± 1.81	-3.48 (-17%)	20.32 ± 1.51	185.06 ± 4.57	+164.74 (+811%)
HI	0.16 ± 0.42	0.20 ± 0.44	+0.04 (+25%)	0.17 ± 0.43	0.27 ± 0.47	+0.10 (+59%)
IO	1.04 ± 0.37	1.42 ± 0.71	+0.38 (+37%)	1.23 ± 0.35	1.02 ± 0.50	-0.21 (-17%)
HIO_2	27.67 ± 3.77	30.36 ± 9.74	+2.69 (+10%)	26.73 ± 5.01	28.12 ± 4.75	+1.39 (+5%)
INO_2	2.30 ± 0.73	1.00 ± 0.58	-1.30 (-57%)	2.36 ± 0.74	1.17 ± 0.50	-1.19 (-50%)
HIO_3	0.79 ± 0.50	0.58 ± 0.64	-0.21 (-27%)	1.02 ± 0.56	0.93 ± 0.63	-0.09 (-9%)
$IONO_2$	6.75 ± 1.39	2.51 ± 1.28	-4.24 (-63%)	6.48 ± 1.57	3.30 ± 1.33	-3.18 (-49%)

For both the T-piece and the guard, the direct signal is comparable in intensity to the signal seen during the HOI calibrations, with the exception of ICl, which is much higher than previously seen. When including the bend into the T-piece experiment, little variation in signal is observed for ICl, HI, IO, HIO_2, and HIO_3, with changes smaller than the standard deviation of the signal. There is a slight decrease in the IBr, INO_2, and $IONO_2$ signal, but the total quantity of loss from these compounds is small compared to the total loss (<4%) The most noticeable loss is observed with HOI, along with an accompanying increase in I_2. When converted into mixing ratios this corresponded to a 42.7 ppt (65%) HOI decrease and a 50.5 ppt (16%) increase in I_2. This conversion of HOI to I_2 likely proceeds via the reverse iodine hydrolysis reaction (R14). The I^- required is most likely from the HOI generation reaction in (R8), which becomes coated on the inlet walls. It is unknown how much I^- is present during field measurements, and so the observed I_2 increase found during the inlet loss tests may be an overestimate compared to atmospheric conditions.

$$HOI + I^- + H^+ \leftrightarrow I_2 + H_2O \quad \text{(R14)}$$

With the salted PTFE guard, a higher proportion of HOI was lost (75% decrease) compared to the T-piece although the amount lost was similar at 43.4 ppt. Meanwhile the proportion of I_2 gain remained about the same (15% increase) but the amount has decreased to 40.0 ppt. There is a marked increase in IBr and ICl signal and the other iodine species remain at similar levels to the T-piece run. Cl^- and Br^- are abundant in sea salt aerosol and are known to react with HOI (Vogt et al., 1999; Braban et al., 2007; Tham et al., 2021), which is the likely reason for the increase in ICl and IBr and further loss of HOI compared to the T-piece experiment. The sensitivities for ICl and IBr have not been measured for Br-CIMS instruments. However, it has been suggested that sensitivities should be similar to that of I_2 (Wang et al., 2021a). If it is assumed that ICl and IBr have the same response to humidity as I_2, the signal change would correspond to a 16.9 and 20.2 ppt increase, respectively. This is far higher than would be expected from the additional HOI loss and may suggest there are additional pathways present to produce ICl and IBr. ~~This again could be from the I^- present from the HOI production step though this likely requires oxidation before reacting with Cl^- and Br^-.~~

3.7 Application to atmospheric HOI and I_2 data~~.~~

I_2 and HOI were measured by the Br-CIMS during the BLEACH campaign in June 2022 with the inlet configuration shown in Fig. ~~6b~~10b. Background signals were measured by flowing dry nitrogen (N_2) through a zero port in the CIMS inlet and through the instrument critical orifice to the IMR, with the rest of the sampled air directed through the sample pump. These zero measurements were repeated hourly, and the signal was linearly interpolated between measurements, providing a value for the background signal during sampling periods. The limit of detection (LoD) for I_2 and HOI were calculated from an extended zeroing period during the campaign as 3 standard deviations of the Allen variance of the zeroing period, similarly to that described in Riva et al. (2024). These corresponded to detection limits of 0.14 ppt for I_2 and 0.27 ppt for HOI.

The HOI calibration could not be performed at dryness, making zero subtraction difficult to quantify. The HOI/I_2 ratio from Fig. 9 could be extrapolated to dryness at the y-intercept which would result in a dry HOI sensitivity that is 1.44 times higher than I_2. However, the 95% confidence interval of the intercept is ±0.43, suggesting a low precision when extrapolating from this calibration. An alternative method is to use the quantum chemical calculations to compare the decay rate between the HOI.Br^- and I_2.Br^- clusters. Using the values from Table 1, the decay rate of HOI.Br^- is slightly slower than I_2.Br^-, which would suggest a slightly higher sensitivity at dryness. However, this value is still similar to the decay rate of I_2.Br^-, and so the dry sensitivity of I_2 could be used as a conservative estimate of the dry HOI sensitivity.

~~The HOI calibration could not be performed at dryness, making zero subtraction difficult to quantify.~~ It ~~wa~~is ~~expected~~ also possible that any signal observed in the zero for HOI and I_2 was due to instrument noise rather than any interferent ~~HOI~~compounds. This was tested by comparing the relative signal intensities of two major isotope peaks of the I_2.Br^- and HOI.Br^- adducts. The theoretical ratios between I_2.$^{79}Br^-$ and I_2.$^{81}Br^-$ and HOI.$^{79}Br^-$ and HOI.$^{81}Br^-$ are~~is~~ 1:0.975 and 1:0.977, respectively. ~~and so t~~The zero data was tested to see whether the ratio between the ~~two~~ isotope peaks were within 10, 20 or 30% of this ratio ~~or whether it fell outside these limits~~. These values are shown in Table ~~2~~3. ~~In total,~~For I_2, 72% of the zero data fell within the 30% ratio limit, suggesting that the signal is generally real and needs to be accounted for by zero subtraction. For HOI, ~~76~~74% of the zero data had isotope ratios that were greater than the 30% tolerance, indicating that the signal generally may not be real. Both the sample and zero timeseries for HOI and I_2 are shown in Fig. A5. The sample timeseries, without zero subtraction, can be considered as an upper limit of the HOI and I_2 mixing ratios.~~and so it was decided to not background subtract the HOI data. Therefore, the HOI data shown should be considered as an upper limit.~~

~~**Table 2: The instrument zero data points during the BLEACH campaign that fell within various limits of the theoretical isotope ratio between the HOI.$^{79}Br^-$ and HOI.$^{81}Br^-$ adduct signals. A ratio value that was greater than 30% of the theoretical value was considered to be outside the ratio tolerance.**~~

	~~Total data points~~	~~Ratio limits~~			
		~~<10%~~	~~<20%~~	~~<30%~~	~~>30%~~
~~Zeroing data~~	~~242~~	~~16~~	~~33~~	~~58~~	~~184~~
	~~(100%)~~	~~(6.6%)~~	~~(13.6%)~~	~~(24.0%)~~	~~(76.0%)~~

Table 3: The instrument zero data points during the BLEACH campaign that fell within various limits of the theoretical isotope ratio between the I_2.Br^- and HOI.Br^- adduct signals. A ratio value that was greater than 30% of the theoretical value was considered to be outside the ratio tolerance.

	Total data points	Ratio limits			
		<10%	<20%	<30%	>30%
I_2 zeroing data	412	129	232	297	115
	(100%)	(31.3%)	(56.3%)	(72.1%)	(27.9%)

Formatted: Caption, Keep with next

Formatted: Centered

Formatted Table

Formatted: Centered

HOI zeroing data	412 (100%)	34 (8.3%)	62 (15.0%)	108 (26.2%)	304 (73.8%)

Formatted: Centered

Measured signals were converted into mixing ratios using the calibrations from Sect. 3.3 and 3.4 and applying the loss corrections described in Sect. 3.5. The ~~I2~~ data was then zero subtracted using the linearly interpolated instrument zeros. Figure ~~8~~ 11 shows the loss-corrected timeseries and diurnal cycles for I_2 and HOI. After zero subtractions and loss corrections, I_2 was detected between 0–0.7 ppt with some mixing ratios dropping to negative values. HOI ranged from 0.~~5~~2 ~~–3.9~~6.0 ppt after its zero subtractions and loss corrections. There was little pattern in the diurnal cycle for I_2 with the average signal being between 0.1–0.3 ppt during both the day and night. The observed mixing ratios of I_2 are similar to previous open ocean measurements at the Cape Verde Atmospheric Observatory of <0.02–0.6 and <0.03–1.67 ppt in May 2007 and 2009 respectively (Lawler et al., 2014). These previous measurements observed a diurnal cycle for I_2 peaking at night, as expected due to its rapid photolysis. A diurnal cycle was not observed in our data, indicating either inlet or background effects which were not adequately quantified by our experiments or an unknown or poorly quantified daytime source of I_2. Potential daytime sources include heterogeneous reactions of photochemically produced oxidants such as HOI with iodide on the surface of aerosols (Vogt et al., 1999; Moon et al., 2026) or on the sea surface (Pound et al., 2024), photochemical oxidation of iodide (Raso et al., 2017) or photochemical reduction of iodate (Reza et al., 2024). However, these would have to be occurring close to the measurement site due to the fast photolytic lifetime of I_2. Additionally, the release of I_2 from aerosol is also a likely contributor to the inlet effects, due to buildup of aerosol on the inlet. With the inlet setup used in this work, these processes are indistinguishable. The overall uncertainty of the I_2 measurements made during the BLEACH campaign, as seen in Sect. 3.7.1, and the fact that they were near to the detection limit of 0.14 ppt means that caution should be applied in interpreting the data.

In contrast, a~~A~~ regular diurnal pattern was observed for HOI, with the signal consistently around 1 ppt during the night and increasing during the day to an average peak of around ~~2.75~~3 ppt. There are no reported mixing ratios of HOI in the open ocean to compare to these values. The closest comparison is to the measurement of HOI at the coastal site of Mace Head (Tham et al., 2021). There, a diurnal cycle was also observed, with low nighttime mixing ratios and an increase during the day. However, the amounts seen at Mace Head during the day were much higher (up to 66.6 ppt), likely due to photochemical reactions caused by I_2 emission by macroalgae (Tham et al., 2021).

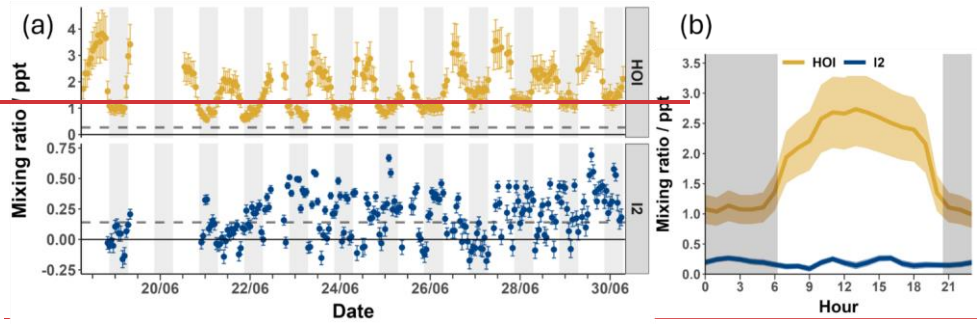

Figure 8: The timeseries (a) and diurnal cycle (b) of the mixing ratios of I_2 (blue) and HOI (yellow) from the BLEACH campaign in June 2022 after zero subtraction (for I_2) and loss correction (for both). The dashed line indicates the limit of

~~detection for each compound. The average relative uncertainty of I_2 was ± 29.6% and for HOI was ± 26.2%~~

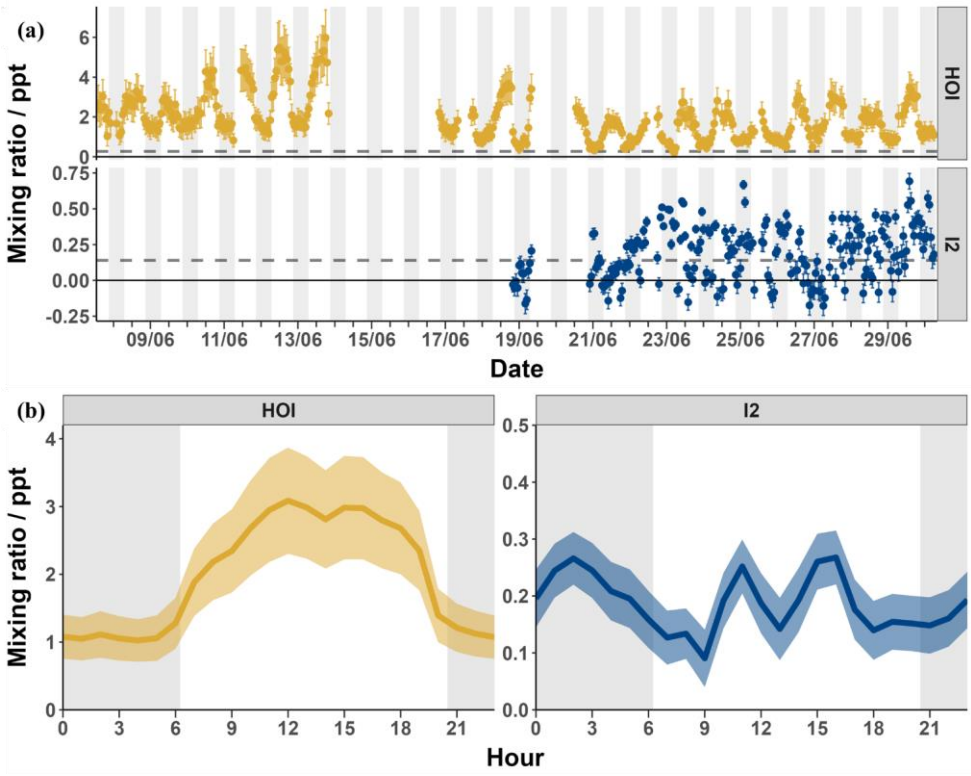

Figure 11: The timeseries (a) and diurnal cycle (b) of the mixing ratios of I_2 (blue) and HOI (yellow) from the BLEACH campaign in June 2022 after zero subtraction and loss correction. The dashed line indicates the limit of detection for each compound. The average relative uncertainty of I_2 was ± 28.7% and for HOI was ± 27.7%.

3.7.1 Measurement uncertainties of atmospheric data

The uncertainty of the I_2 and HOI mixing ratios were again calculated by propagation of uncertainty. ~~For I_2, t~~This was calculated from the uncertainty of the humidity independent sensitivity, twice the uncertainty of the dry sensitivity from the linear interpolation calculation, and the uncertainty of the instrument signal during the inlet loss experiment. This resulted in an average relative error throughout the BLEACH campaign of ~~29.6~~28.7% for I_2 and 27.7% for HOI. There are a number of other uncertainties from the inlet loss experiment that cannot be quantified and so the uncertainty for I_2 and HOI should be

considered a lower limit. In future work, repeated experiments may be able to account for these uncertainties by finding a standard deviation of the loss correction value.

~~The uncertainty of HOI was calculated with just the uncertainty from the humidity dependent sensitivity and the uncertainty of the instrument signal during the inlet loss experiment, resulting in an average relative error of 26.2% throughout the BLEACH campaign. The HOI uncertainty value should also be considered a lower limit as there are the other unquantified uncertainties of the inlet loss experiment and a lack of a zero subtraction.~~

4. Summary and conclusions

There have been few atmospheric measurements of HOI and I_2 due to the requirement of highly sensitive and selective instrumentation and the lack of readily available calibration methods for HOI. In this study, we demonstrate a novel method for the generation and calibration of HOI at ppt levels, utilising its interconversion to I_2 via chemical traps. The presence of potential interferent iodine compounds was found to be negligible and the calibration was shown to be repeatable over a range of humidities. The developed calibration method was utilised to ascertain the humidity dependence of the CIMS for HOI and I_2. It was found that at humidities typical of the marine boundary layer, I_2 exhibited a humidity-independent sensitivity whereas HOI showed a slight negative dependency. A possible explanation, supported by QRRK theory, is that higher humidities increase the proportion of the $Br(H_2O)^-$ reagent ion, which has a lower adduct formation enthalpy with HOI and I_2 compared to the Br^- reagent ion, resulting in decreased sensitivities. However, the presence of H_2O increases the available ~~harmonic oscillators~~vibrational modes of the adduct, improving the energy distribution and stabilisation of the adduct and increasing its sensitivity. This effect is greater for $I_2.Br^-$ as it has fewer harmonic oscillators than $HOI.Br^-$ and these two opposing factors mean that the sensitivity of $I_2.Br^-$ is humidity independent. However, this stabilisation is not sufficient in the case of the $HOI.Br^-$ adduct to mitigate the increasing proportion of $Br(H_2O)^-$ vs Br^- reagent ions, resulting in a decreased sensitivity at high humidities.

Heterogeneous chemistry and inlet wall losses are a perennial problem in the measurement of acidic and reactive species, which can be exacerbated depending on the inlet configuration. When using the inlet configuration made for field measurements, up to 75% of the HOI signal was lost compared to the calibration setup. This was accompanied by a corresponding increase in I_2 signal, suggesting that this loss occurred via the reverse hydrolysis of iodine.

After correcting for humidity sensitivities and inlet losses, we detected I_2 and HOI in the marine boundary layer during the BLEACH campaign at Tudor Hill, Bermuda in June 2022 at mixing ratios of between 0–0.7 ppt for I_2 and ~~an upper limit of~~ 0.~~5~~2–~~6.0~~3.~~8~~ ppt for HOI. The overall uncertainty of these measurements was calculated as ± ~~29.6~~28.7% for I_2 and ± ~~26.3~~27.7% for HOI. These uncertainties can be considered as lower limits as there were additional uncertainties from the inlet loss

experiment that were not quantifiable. ~~Additionally, zero subtraction could not be performed for the HOI data which could further increase the relative error.~~

In future work, the accuracy for I_2 and HOI could be improved by performing background measurements at similar humidity levels to the ambient measurements, reducing the need to account for large differences in sensitivities from different humidities. Additionally, further work on the HOI calibration can further constrain the uncertainty of the humidity dependent HOI/I_2 ratio over a wider range of humidities. Finally, development of atmospheric detection of HOI and I_2 should focus on using instrument inlets that can minimise inlet effects for these compounds, reducing the need to perform correction tests. Any correction tests that are performed should be done before, during, and after field measurement collection to best characterise any inlet artifacts and changes during the measurements.

Appendix

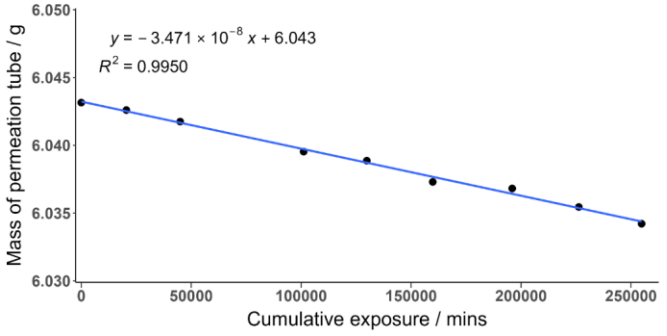

Figure A1: The mass loss of an I_2 permeation tube over time. The gradient represents the emission rate of the permeation tube. Each data point is the average of 6 measurements.

Formatted: Normal

Formatted: Keep with next

Formatted: Subscript

Formatted: Normal

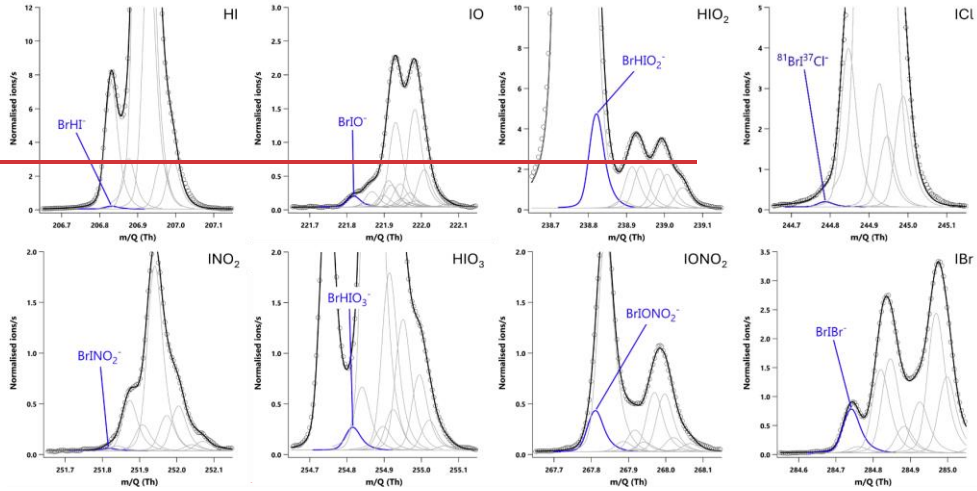

Figure A1: 20-minute averaged high resolution single peak mass spectra fits for potential iodine containing compounds during the HOI calibrations with the NaI trap in place.

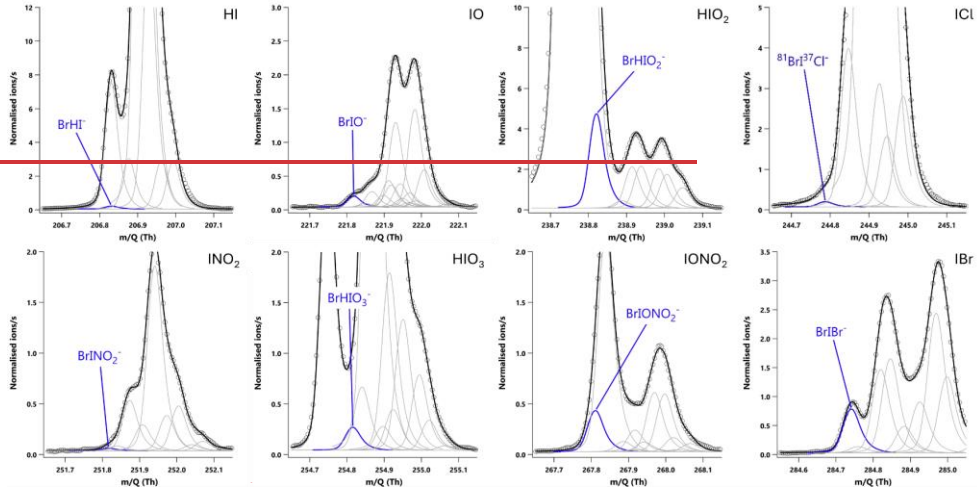

Figure A2: 20-minute averaged high resolution single peak mass spectra fits for potential iodine containing compounds during the HOI calibrations after the removal of the NaI trap.

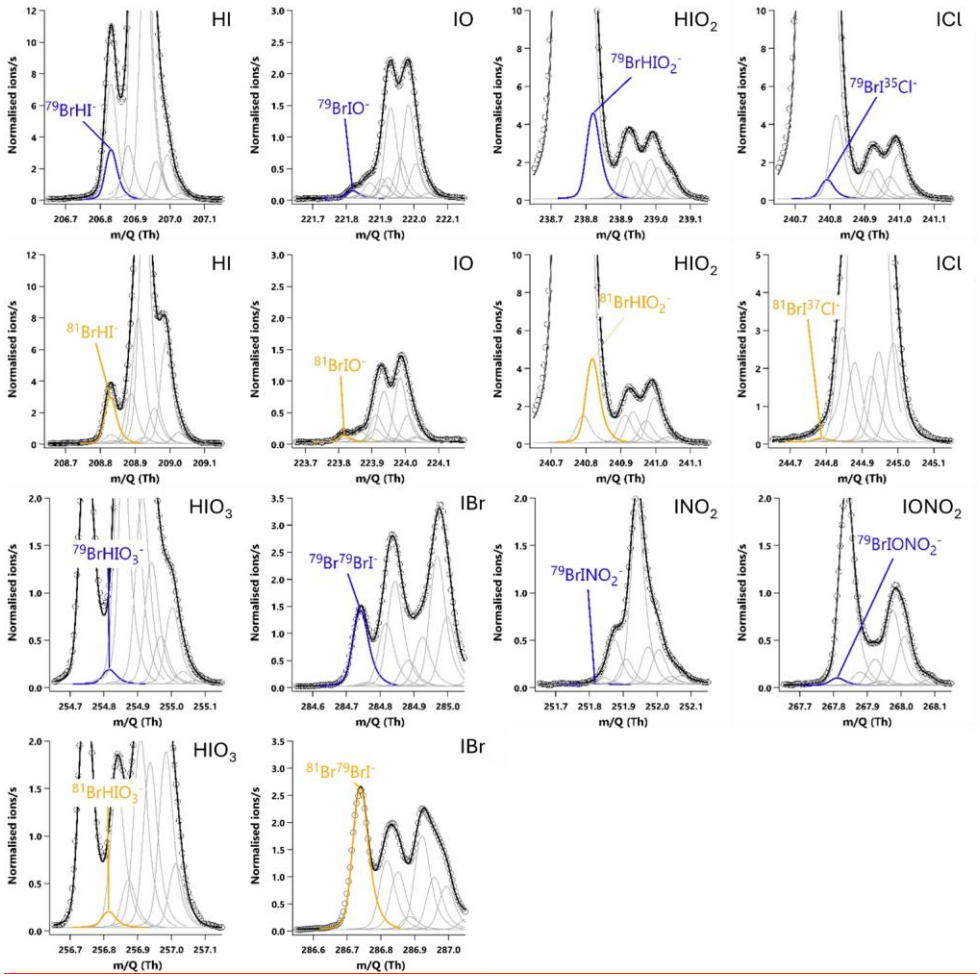

Figure A2: 20-minute averaged high resolution single peak mass spectra fits for potential iodine containing compounds during the HOI calibrations with the NaI trap in place. The molecular ion peak is shown in blue with the primary isotope peak in gold with an exception for $^{81}Br^{37}Cl^-$ as this was the isotope used to calculate the BrICl signal. Isotope peak shapes were determined using the Tofware software. The isotope peaks of $BrINO_2^-$ and $BrIONO_2^-$ were not able to be visualised by the software.

Formatted: Keep with next

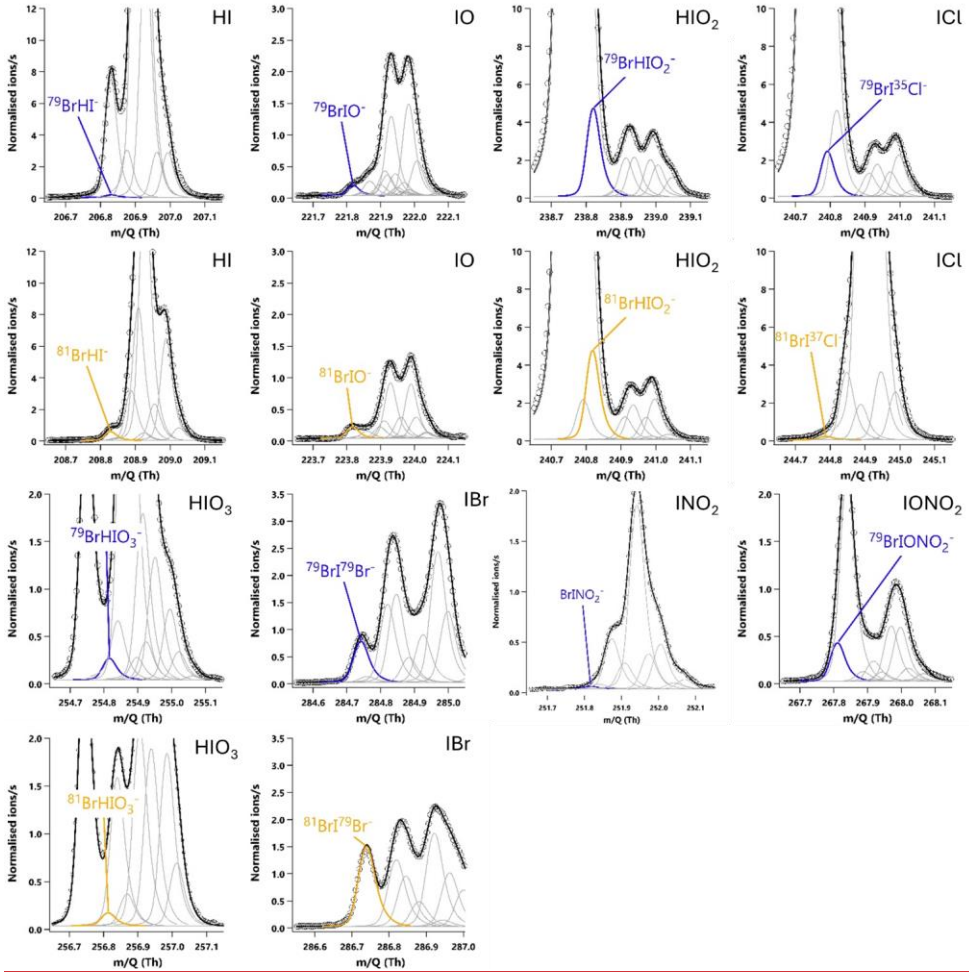

Figure A3: 20-minute averaged high resolution single peak mass spectra fits for potential iodine containing compounds during the HOI calibrations after the removal of the NaI trap. The molecular ion peak is shown in blue with the primary isotope peak in gold with an exception for $^{81}Br^{37}Cl^-$ as this was the isotope used to calculate the BrICl signal. Isotope peak shapes were determined using the Tofware software. The isotope peaks of $BrINO_2^-$ and $BrIONO_2^-$ were not able to be visualised by the software.

Formatted: Keep with next

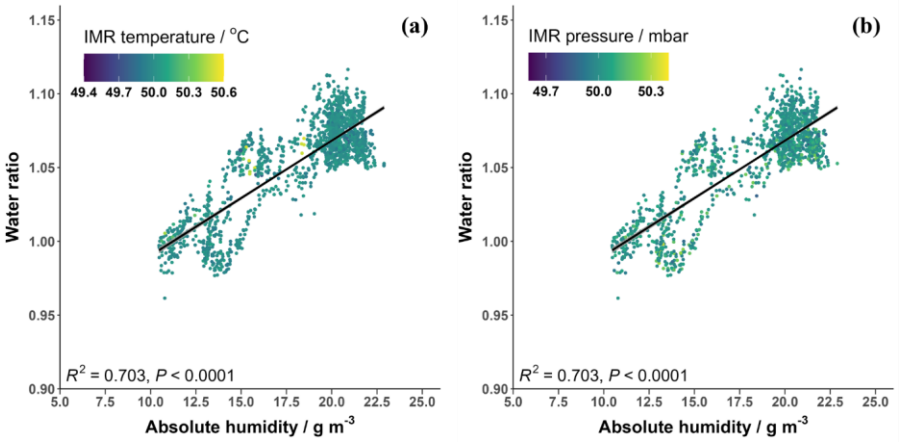

Figure A4: The water ratio in the CIMS IMR plotted against the absolute humidity measured during the BLEACH campaign coloured by (a) the variation in IMR temperature and (b) the variation in IMR pressure.

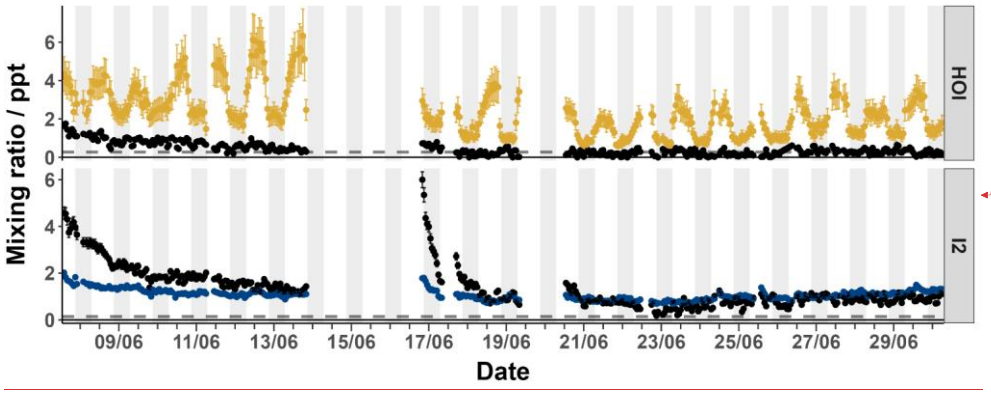

Figure A5: The timeseries of the sample mixing ratios of HOI (yellow) and I_2 (blue) along with their corresponding zero mixing ratios (black) from the BLEACH campaign in June 2022. The dashed line indicates the limit of detection for each compound.

Formatted: Keep with next

Formatted: Font color: Auto

Formatted: Normal

Formatted: Keep with next

Formatted: Caption

Table A1: The signal change (in normalised ion counts per second) of HNO_3, HI, IBr and I_2 along with their calculated standard errors during the HOI calibration runs upon addition of the NaI trap.

Run number	Signal change (± standard error) on addition of NaI trap / ncps			
	HNO_3	HI	IBr	I_2
1	-4902.1 (± 71.5)	36.49 (± 0.93)	6.84 (± 0.51)	430.04 (± 10.89)
2	-5274.0 (± 164.4)	20.25 (± 0.80)	5.07 (± 0.46)	451.62 (± 13.60)
3	-4543.7 (± 43.7)	11.96 (± 0.69)	4.73 (± 0.40)	519.53 (±5.76)
4	-4129.3 (± 58.4)	10.72 (± 1.02)	5.82 (± 0.49)	573.95 (±6.90)
5	-4051.3 (± 116.0)	13.98 (± 1.41)	7.24 (± 0.51)	517.84 (±8.79)
6	-4865.5 (± 48.7)	6.77 (± 0.95)	6.98 (± 0.53)	662.69 (±9.09)
7	-2812.2 (± 43.3)	6.57 (± 0.82)	10.66 (± 0.52)	424.65 (±6.39)
8	-3742.2 (± 64.4)	24.76 (± 1.09)	6.89 (± 0.49)	391.72 (±5.24)
9	-2413.3 (± 63.5)	6.67 (± 0.55)	11.63 (± 0.55)	553.02 (±7.72)
10	-4725.2 (± 50.5)	4.26 (± 0.82)	7.35 (± 0.40)	516.05 (±4.749)
11	-4555.5 (± 52.7)	2.27 (± 0.48)	8.04 (± 0.40)	884.80 (±7.62)

Data availability

Datasets for the figures shown are available at: https://doi.org/10.15124/48ade8f3-d750-4fe6-a2d9-b8f69bf86262

Author contribution

LM, MS, LJC and SJA designed and developed the humidity dependence calibrations for I_2 which were conducted by LM. MS, PR and JT developed the HOI calibration method and was adapted and conducted in lab experiments by LM and MZ. BA was responsible for the management and coordination of the BLEACH field campaign and AP was responsible for the management and usage of the Tudor Hill Marine Atmospheric Observatory.
PBK performed the quantum chemical calculations.
LM and LJC prepared the paper, and all authors reviewed the paper.

Competing interests

The authors declare that they have no conflict of interest.

Acknowledgements

The authors would like to thank John Halfacre, William Drysdale, Allison Moon, Alyson Fritzmann and Gordon Novak for their help during the BLEACH summer campaign.

Financial support

This research was supported by the European Research Council, Horizon Europe European Research Council (grant no. 833290).
BA, JT and PR were supported by NSF AGS 2109323
The Tudor Hill Marine Atmospheric Observatory was supported by the National Science Foundation's Chemical Oceanography Program, grant OCE-2123053.

References

Auzmendi-Murua, I., Castillo, A., and Bozzelli, J.: Mercury Oxidation via Chlorine, Bromine, and Iodine under Atmospheric Conditions: Thermochemistry and Kinetics, JOURNAL OF PHYSICAL CHEMISTRY A, 118, 2959-2975, 10.1021/jp412654s, 2014.

Bitter, M., Ball, S., Povey, I., and Jones, R.: A broadband cavity ringdown spectrometer for in-situ measurements of atmospheric trace gases, ATMOSPHERIC CHEMISTRY AND PHYSICS, 5, 2547-2560, 2005.

Breitenlechner, M., Novak, G., Neuman, J., Rollins, A., and Veres, P.: A versatile vacuum ultraviolet ion source for reduced pressure bipolar chemical ionization mass spectrometry, ATMOSPHERIC MEASUREMENT TECHNIQUES, 15, 1159-1169, 10.5194/amt-15-1159-2022, 2022.

Buys, Z., Brough, N., Huey, L., Tanner, D., von Glasow, R., and Jones, A.: High temporal resolution Br2, BrCl and BrO observations in coastal Antarctica, ATMOSPHERIC CHEMISTRY AND PHYSICS, 13, 1329-1343, 10.5194/acp-13-1329-2013, 2013.

Calvert, J. G. and Lindberg, S. E.: The potential influence of iodine-containing compounds on the chemistry of the troposphere in the polar spring. II. Mercury depletion, Atmospheric Environment, 38, 5105-5116, 10.1016/j.atmosenv.2004.05.050, 2004.

Caram, C., Szopa, S., Cozic, A., Bekki, S., Cuevas, C., and Saiz-Lopez, A.: Sensitivity of tropospheric ozone to halogen chemistry in thechemistry-climate model LMDZ-INCA vNMHC, GEOSCIENTIFIC MODEL DEVELOPMENT, 16, 4041-4062, 10.5194/gmd-16-4041-2023, 2023.

Carpenter, L. J., MacDonald, S. M., Shaw, M. D., Kumar, R., Saunders, R. W., Parthipan, R., Wilson, J., and Plane, J. M. C.: Atmospheric iodine levels influenced by sea surface emissions of inorganic iodine, Nature Geoscience, 6, 108-111, 10.1038/ngeo1687, 2013.

Chameides, W. L. and Davis, D. D.: IODINE - ITS POSSIBLE ROLE IN TROPOSPHERIC PHOTOCHEMISTRY, Journal of Geophysical Research-Oceans, 85, 7383-7398, 10.1029/JC085iC12p07383, 1980.

Cuevas, C. A., Maffezzoli, N., Corella, J. P., Spolaor, A., Vallelonga, P., Kjaer, H. A., Simonsen, M., Winstrup, M., Vinther, B., Horvat, C., Fernandez, R. P., Kinnison, D., Lamarque, J. F., Barbante, C., and Saiz-Lopez, A.: Rapid increase in atmospheric iodine levels in the North Atlantic since the mid-20th century, Nature Communications, 9, 6, 10.1038/s41467-018-03756-1, 2018.

Custard, K., Pratt, K., Wang, S., and Shepson, P.: Constraints on Arctic Atmospheric Chlorine Production through Measurements and Simulations of Cl₂ and ClO, ENVIRONMENTAL SCIENCE & TECHNOLOGY, 50, 12394-12400, 10.1021/acs.est.6b03909, 2016.

Deming, B., Pagonis, D., Liu, X., Day, D., Talukdar, R., Krechmer, J., de Gouw, J., Jimenez, J., and Ziemann, P.: Measurements of delays of gas-phase compounds in a wide variety of tubing materials due to gas-wall interactions, ATMOSPHERIC MEASUREMENT TECHNIQUES, 12, 3453-3461, 10.5194/amt-12-3453-2019, 2019.

Dörich, R., Eger, P., Lelieveld, J., and Crowley, J.: Iodide CIMS and m/z 62: the detection of HNO3 as NO3- in the presence of PAN, peroxyacetic acid and ozone, ATMOSPHERIC MEASUREMENT TECHNIQUES, 14, 5319-5332, 10.5194/amt-14-5319-2021, 2021.

Finkenzeller, H., Iyer, S., He, X., Simon, M., Koenig, T., Lee, C., Valiev, R., Hofbauer, V., Amorim, A., Baalbaki, R., Baccarini, A., Beck, L., Bell, D., Caudillo, L., Chen, D., Chiu, R., Chu, B., Dada, L., Duplissy, J., ..., and Volkamer, R.: The gas-phase formation mechanism of iodic acid as an atmospheric aerosol source, NATURE CHEMISTRY, 15, 129-+, 10.1038/s41557-022-01067-z, 2023.

Frisch, M. J., Trucks, G. W., Schlegel, H. B., Scuseria, G. E., Robb, M. A., Cheeseman, J. R., Scalmani, G., Barone, V., Petersson, G. A., Nakatsuji, H., Li, X., Caricato, M., Marenich, A. V., Bloino, J., Janesko, B. G., Gomperts, R., Mennucci, B., Hratchian, H. P., Ortiz, J. V., ..., and Fox, D. J.: Gaussian 16 Rev. C.02 [code], 2019.

Garland, J. A., Elzerman, A. W., and Penkett, S. A.: THE MECHANISM FOR DRY DEPOSITION OF OZONE TO SEAWATER SURFACES, Journal of Geophysical Research-Oceans, 85, 7488-7492, 10.1029/JC085iC12p07488, 1980.

He, X., Shen, J., Iyer, S., Juuti, P., Zhang, J., Koirala, M., Kytökari, M., Worsnop, D., Rissanen, M., Kulmala, M., Maier, N., Mikkilä, J., Sipilä, M., and Kangasluoma, J.: Characterisation of gaseous iodine species detection using the multi-scheme

Formatted: EndNote Bibliography

chemical ionisation inlet 2 with bromide and nitrate chemical ionisation methods, ATMOSPHERIC MEASUREMENT TECHNIQUES, 16, 4461-4487, 10.5194/amt-16-4461-2023, 2023.
Huang, R., Seitz, K., Buxmann, J., Pöhler, D., Hornsby, K., Carpenter, L., Platt, U., and Hoffmann, T.: In situ measurements of molecular iodine in the marine boundary layer: the link to macroalgae and the implications for O₃, IO, OIO and NO_x, ATMOSPHERIC CHEMISTRY AND PHYSICS, 10, 4823-4833, 10.5194/acp-10-4823-2010, 2010.
Huang, Y., Zhao, R., Charan, S., Kenseth, C., Zhang, X., and Seinfeld, J.: Unified Theory of Vapor-Wall Mass Transport in Teflon-Walled Environmental Chambers, ENVIRONMENTAL SCIENCE & TECHNOLOGY, 52, 2134-2142, 10.1021/acs.est.7b05575, 2018.
Huey, L.: Measurement of trace atmospheric species by chemical ionization mass spectrometry: Speciation of reactive nitrogen and future directions, MASS SPECTROMETRY REVIEWS, 26, 166-184, 10.1002/mas.20118, 2007.
Iglesias-Suarez, F., Badia, A., Fernandez, R. P., Cuevas, C. A., Kinnison, D. E., Tilmes, S., Lamarque, J. F., Long, M. C., Hossaini, R., and Saiz-Lopez, A.: Natural halogens buffer tropospheric ozone in a changing climate, Nature Climate Change, 10, 147-+, 10.1038/s41558-019-0675-6, 2020.
Iyer, S., Lopez-Hilfiker, F., Lee, B., Thornton, J., and Kurtén, T.: Modeling the Detection of Organic and Inorganic Compounds Using Iodide-Based Chemical Ionization, JOURNAL OF PHYSICAL CHEMISTRY A, 120, 576-587, 10.1021/acs.jpca.5b09837, 2016.
Ji, Y., Huey, G., Tanner, D. J., Lee, Y. R., Veres, P. R., Neuman, J. A., Wang, Y. H., and Wang, X. M.: A vacuum ultraviolet ion source (VUV-IS) for iodide-chemical ionization mass spectrometry: a substitute for radioactive ion sources, Atmospheric Measurement Techniques, 13, 3683-3696, 10.5194/amt-13-3683-2020, 2020.
Kassel, L. S.: Studies in homogeneous gas reactions II Introduction of quantum theory, Journal of Physical Chemistry, 32, 1065-1079, 10.1021/j150289a011, 1928.
Kercher, J. P., Riedel, T. P., and Thornton, J. A.: Chlorine activation by N₂O₅: simultaneous, in situ detection of ClNO₂ and N₂O₅ by chemical ionization mass spectrometry, Atmospheric Measurement Techniques, 2, 193-204, 10.5194/amt-2-193-2009, 2009.
Klobas, J., Hansen, J., Weisenstein, D., Kennedy, R., and Wilmouth, D.: Sensitivity of Iodine-Mediated Stratospheric Ozone Loss Chemistry to Future Chemistry-Climate Scenarios, FRONTIERS IN EARTH SCIENCE, 9, 10.3389/feart.2021.617586, 2021.
Koenig, T., Baidar, S., Campuzano-Jost, P., Cuevas, C., Dix, B., Fernandez, R., Guo, H., Hall, S., Kinnison, D., Nault, B., Ullmann, K., Jimenez, J., Saiz-Lopez, A., and Volkamer, R.: Quantitative detection of iodine in the stratosphere, PROCEEDINGS OF THE NATIONAL ACADEMY OF SCIENCES OF THE UNITED STATES OF AMERICA, 117, 1860-1866, 10.1073/pnas.1916828117, 2020.
Krechmer, J., Pagonis, D., Ziemann, P., and Jimenez, J.: Quantification of Gas-Wall Partitioning in Teflon Environmental Chambers Using Rapid Bursts of Low-Volatility Oxidized Species Generated in Situ, ENVIRONMENTAL SCIENCE & TECHNOLOGY, 50, 5757-5765, 10.1021/acs.est.6b00606, 2016.
Kurtén, T., Kuang, C. A., Gómez, P., McMurry, P. H., Vehkamäki, H., Ortega, I., Noppel, M., and Kulmala, M.: The role of cluster energy nonaccommodation in atmospheric sulfuric acid nucleation, Journal of Chemical Physics, 132, 8, 10.1063/1.3291213, 2010.
Laidler, K.: Chemical Kinetics, 3rd, Harper & Row, 531 pp.1987.
Lawler, M., Mahajan, A., Saiz-Lopez, A., and Saltzman, E.: Observations of I₂ at a remote marine site, ATMOSPHERIC CHEMISTRY AND PHYSICS, 14, 2669-2678, 10.5194/acp-14-2669-2014, 2014.
Lawler, M. J., Sander, R., Carpenter, L. J., Lee, J. D., Von Glasow, R., Sommariva, R., and Saltzman, E. S.: HOCl and Cl₂ observations in marine air, Atmospheric Chemistry and Physics, 11, 7617-7628, 10.5194/acp-11-7617-2011, 2011.
Le Breton, M., Bannan, T., Shallcross, D., Khan, M., Evans, M., Lee, J., Lidster, R., Andrews, S., Carpenter, L., Schmidt, J., Jacob, D., Harris, N., Bauguitte, S., Gallagher, M., Bacak, A., Leather, K., and Percival, C.: Enhanced ozone loss by active inorganic bromine chemistry in the tropical troposphere, ATMOSPHERIC ENVIRONMENT, 155, 21-28, 10.1016/j.atmosenv.2017.02.003, 2017.
Lee, B., Lopez-Hilfiker, F., Veres, P., McDuffie, E., Fibiger, D., Sparks, T., Ebben, C., Green, J., Schroder, J., Campuzano-Jost, P., Iyer, S., D'Ambro, E., Schobesberger, S., Brown, S., Wooldridge, P., Cohen, R., Fiddler, M., Bililign, S., Jimenez, J., ..., and Thornton, J.: Flight Deployment of a High-Resolution Time-of-Flight Chemical Ionization Mass Spectrometer:

Observations of Reactive Halogen and Nitrogen Oxide Species, JOURNAL OF GEOPHYSICAL RESEARCH-ATMOSPHERES, 123, 7670-7686, 10.1029/2017JD028082, 2018.
Lee, B. H., Lopez-Hilfiker, F. D., Mohr, C., Kurtén, T., Worsnop, D. R., and Thornton, J. A.: An Iodide-Adduct High-Resolution Time-of-Flight Chemical-Ionization Mass Spectrometer: Application to Atmospheric Inorganic and Organic Compounds, Environmental Science & Technology, 48, 6309-6317, 10.1021/es500362a, 2014.
Lee, C., Elgiar, T., David, L., Wilmot, T., Reza, M., Hirshorn, N., McCubbin, I., Shah, V., Lin, J., Lyman, S., Hallar, A., Gratz, L., and Volkamer, R.: Elevated Tropospheric Iodine Over the Central Continental United States: Is Iodine a Major Oxidant of Atmospheric Mercury?, GEOPHYSICAL RESEARCH LETTERS, 51, 10.1029/2024GL109247, 2024.
Legrand, M., McConnell, J., Preunkert, S., Arienzo, M., Chellman, N., Gleason, K., Sherwen, T., Evans, M., and Carpenter, L.: Alpine ice evidence of a three-fold increase in atmospheric iodine deposition since 1950 in Europe due to increasing oceanic emissions, PROCEEDINGS OF THE NATIONAL ACADEMY OF SCIENCES OF THE UNITED STATES OF AMERICA, 115, 12136-12141, 10.1073/pnas.1809867115, 2018.
Liao, J., Huey, L., Liu, Z., Tanner, D., Cantrell, C., Orlando, J., Flocke, F., Shepson, P., Weinheimer, A., Hall, S., Ullmann, K., Beine, H., Wang, Y., Ingall, E., Stephens, C., Hornbrook, R., Apel, E., Riemer, D., Fried, A., ..., and Nowak, J.: High levels of molecular chlorine in the Arctic atmosphere, NATURE GEOSCIENCE, 7, 91-94, 10.1038/NGEO2046, 2014.
Liao, J., Huey, L. G., Scheuer, E., Dibb, J. E., Stickel, R. E., Tanner, D. J., Neuman, J. A., Nowak, J. B., Choi, S., Wang, Y., Salawitch, R. J., Canty, T., Chance, K., Kurosu, T., Suleiman, R., Weinheimer, A. J., Shetter, R. E., Fried, A., Brune, W., ..., and Ingall, E. D.: Characterization of soluble bromide measurements and a case study of BrO observations during ARCTAS, Atmospheric Chemistry and Physics, 12, 1327-1338, 10.5194/acp-12-1327-2012, 2012.
MacDonald, S., Martín, J., Chance, R., Warriner, S., Saiz-Lopez, A., Carpenter, L., and Plane, J.: A laboratory characterisation of inorganic iodine emissions from the sea surface: dependence on oceanic variables and parameterisation for global modelling, ATMOSPHERIC CHEMISTRY AND PHYSICS, 14, 5841-5852, 10.5194/acp-14-5841-2014, 2014.
Mahajan, A., Oetjen, H., Saiz-Lopez, A., Lee, J., McFiggans, G., and Plane, J.: Reactive iodine species in a semi-polluted environment, GEOPHYSICAL RESEARCH LETTERS, 36, 10.1029/2009GL038018, 2009.
Marcy, T., Gao, R., Northway, M., Popp, P., Stark, H., and Fahey, D.: Using chemical ionization mass spectrometry for detection of HNO3, HOl, and ClONO2 in the atmosphere, INTERNATIONAL JOURNAL OF MASS SPECTROMETRY, 243, 63-70, 10.1016/j.ijms.2004.11.012, 2005.
Moon, A., Liu, L., Wang, X., Chan, Y., Fritzmann, A., Pound, R., Lees, A., Marden, L., Evans, M., Carpenter, L., Stutz, J., Thornton, J., Novak, G., Rollins, A., Schill, G., He, X., Finkenzeller, H., Reza, M., Volkamer, R., ..., and Alexander, B.: Aerosol iodine recycling is a major control on tropospheric reactive iodine abundance, ATMOSPHERIC CHEMISTRY AND PHYSICS, 26, 2353-2389, 10.5194/acp-26-2353-2026, 2026.
Neale, P., Hylander, S., Banaszak, A., Häder, D., Rose, K., Vione, D., Wängberg, S., Jansen, M., Busquets, R., Andersen, M., Madronich, S., Hanson, M., Schikowski, T., Solomon, K., Sulzberger, B., Wallington, T., Heikkilä, A., Pandey, K., Andrady, A., ..., and Zepp, R.: Environmental consequences of interacting effects of changes in stratospheric ozone, ultraviolet radiation, and climate: UNEP Environmental Effects Assessment Panel, Update 2024, PHOTOCHEMICAL & PHOTOBIOLOGICAL SCIENCES, 24, 357-392, 10.1007/s43630-025-00687-x, 2025.
Neuman, J., Nowak, J., Huey, L., Burkholder, J., Dibb, J., Holloway, J., Liao, J., Peischl, J., Roberts, J., Ryerson, T., Scheuer, E., Stark, H., Stickel, R., Tanner, D., and Weinheimer, A.: Bromine measurements in ozone depleted air over the Arctic Ocean, ATMOSPHERIC CHEMISTRY AND PHYSICS, 10, 6503-6514, 10.5194/acp-10-6503-2010, 2010.
O'Dowd, C., Hämeri, K., Mäkelä, J., Väkeva, M., Aalto, P., de Leeuw, G., Kunz, G., Becker, E., Hansson, H., Allen, A., Harrison, R., Berresheim, H., Geever, M., Jennings, S., and Kulmala, M.: Coastal new particle formation:: Environmental conditions and aerosol physicochemical characteristics during nucleation bursts -: art. no. 8107, JOURNAL OF GEOPHYSICAL RESEARCH-ATMOSPHERES, 107, 10.1029/2000JD000206, 2002.
Peng, X., Wang, T., Wang, W., Ravishankara, A., George, C., Xia, M., Cai, M., Li, Q., Salvador, C., Lau, C., Lyu, X., Poon, C., Mellouki, A., Mu, Y., Hallquist, M., Saiz-Lopez, A., Guo, H., Herrmann, H., Yu, C., ..., and Chen, J.: Photodissociation of particulate nitrate as a source of daytime tropospheric Cl₂, NATURE COMMUNICATIONS, 13, 10.1038/s41467-022-28383-9, 2022.
Peters, C., Pechtl, S., Stutz, J., Hebestreit, K., Hönninger, G., Heumann, K., Schwarz, A., Winterlik, J., and Platt, U.: Reactive and organic halogen species in three different European coastal environments, ATMOSPHERIC CHEMISTRY AND PHYSICS, 5, 3357-3375, 2005.

Pound, R., Brown, L., Evans, M., and Carpenter, L.: An improved estimate of inorganic iodine emissions from the ocean using a coupled surface microlayer box model, ATMOSPHERIC CHEMISTRY AND PHYSICS, 24, 9899-9921, 10.5194/acp-24-9899-2024, 2024.
Pound, R., Durcan, D., Evans, M., and Carpenter, L.: Comparing the Importance of Iodine and Isoprene on Tropospheric Photochemistry, GEOPHYSICAL RESEARCH LETTERS, 50, 10.1029/2022GL100997, 2023.
Prados-Roman, C., Cuevas, C., Hay, T., Fernandez, R., Mahajan, A., Royer, S., Galí, M., Simó, R., Dachs, J., Grossmann, K., Kinnison, D., Lamarque, J., and Saiz-Lopez, A.: Iodine oxide in the global marine boundary layer, ATMOSPHERIC CHEMISTRY AND PHYSICS, 15, 583-593, 10.5194/acp-15-583-2015, 2015.
Priestley, M., le Breton, M., Bannan, T., Worrall, S., Bacak, A., Smedley, A., Reyes-Villegas, E., Mehra, A., Allan, J., Webb, A., Shallcross, D., Coe, H., and Percival, C.: Observations of organic and inorganic chlorinated compounds and their contribution to chlorine radical concentrations in an urban environment in northern Europe during the wintertime, ATMOSPHERIC CHEMISTRY AND PHYSICS, 18, 13481-13493, 10.5194/acp-18-13481-2018, 2018.
Pritchard, B., Altarawy, D., Didier, B., Gibson, T., and Windus, T.: New Basis Set Exchange: An Open, Up-to-Date Resource for the Molecular Sciences Community, JOURNAL OF CHEMICAL INFORMATION AND MODELING, 59, 4814-4820, 10.1021/acs.jcim.9b00725, 2019.
Raso, A., Custard, K., May, N., Tanner, D., Newburn, M., Walker, L., Moore, R., Huey, L., Alexander, L., Shepson, P., and Pratt, K.: Active molecular iodine photochemistry in the Arctic, PROCEEDINGS OF THE NATIONAL ACADEMY OF SCIENCES OF THE UNITED STATES OF AMERICA, 114, 10053-10058, 10.1073/pnas.1702803114, 2017.
Read, K. A., Mahajan, A. S., Carpenter, L. J., Evans, M. J., Faria, B. V. E., Heard, D. E., Hopkins, J. R., Lee, J. D., Moller, S. J., Lewis, A. C., Mendes, L., McQuaid, J. B., Oetjen, H., Saiz-Lopez, A., Pilling, M. J., and Plane, J. M. C.: Extensive halogen-mediated ozone destruction over the tropical Atlantic Ocean, Nature, 453, 1232-1235, 10.1038/nature07035, 2008.
Reza, M., Iezzi, L., Finkenzeller, H., Roose, A., Ammann, M., and Volkamer, R.: Iodine Activation from Iodate Reduction in Aqueous Films via Photocatalyzed and Dark Reactions, ACS EARTH AND SPACE CHEMISTRY, 8, 2495-2508, 10.1021/acsearthspacechem.4c00224, 2024.
Rice, O. K. and Ramsperger, H. C.: Theories of unimolecular gas reactions at low pressures, Journal of the American Chemical Society, 49, 1617-1629, 10.1021/ja01406a001, 1927.
Rissanen, M., Mikkilä, J., Iyer, S., and Hakala, J.: Multi-scheme chemical ionization inlet (MION) for fast switching of reagent ion chemistry in atmospheric pressure chemical ionization mass spectrometry (CIMS) applications, ATMOSPHERIC MEASUREMENT TECHNIQUES, 12, 6635-6646, 10.5194/amt-12-6635-2019, 2019.
Riva, M., Pospisilova, V., Frege, C., Perrier, S., Bansal, P., Jorga, S., Sturm, P., Thornton, J., Rohner, U., and Lopez-Hilfiker, F.: Evaluation of a reduced-pressure chemical ion reactor utilizing adduct ionization for the detection of gaseous organic and inorganic species, ATMOSPHERIC MEASUREMENT TECHNIQUES, 17, 5887-5901, 10.5194/amt-17-5887-2024, 2024.
Robinson, M., Neuman, J., Huey, L., Roberts, J., Brown, S., and Veres, P.: Temperature-dependent sensitivity of iodide chemical ionization mass spectrometers, ATMOSPHERIC MEASUREMENT TECHNIQUES, 15, 4295-4305, 10.5194/amt-15-4295-2022, 2022.
Roscoe, H., Brough, N., Jones, A., Wittrock, F., Richter, A., Van Roozendael, M., and Hendrick, F.: Characterisation of vertical BrO distribution during events of enhanced tropospheric BrO in Antarctica, from combined remote and in-situ measurements, JOURNAL OF QUANTITATIVE SPECTROSCOPY & RADIATIVE TRANSFER, 138, 70-81, 10.1016/j.jqsrt.2014.01.026, 2014.
Saiz-Lopez, A. and Plane, J.: Novel iodine chemistry in the marine boundary layer, GEOPHYSICAL RESEARCH LETTERS, 31, 10.1029/2003GL019215, 2004.
Saiz-Lopez, A. and von Glasow, R.: Reactive halogen chemistry in the troposphere, CHEMICAL SOCIETY REVIEWS, 41, 6448-6472, 10.1039/c2cs35208g, 2012.
Saiz-Lopez, A., Fernandez, R. P., Ordonez, C., Kinnison, D. E., Martin, J. C. G., Lamarque, J. F., and Tilmes, S.: Iodine chemistry in the troposphere and its effect on ozone, Atmospheric Chemistry and Physics, 14, 13119-13143, 10.5194/acp-14-13119-2014, 2014.
Saiz-Lopez, A., Plane, J. M. C., Baker, A. R., Carpenter, L. J., von Glasow, R., Martin, J. C. G., McFiggans, G., and Saunders, R. W.: Atmospheric Chemistry of Iodine, Chemical Reviews, 112, 1773-1804, 10.1021/cr200029u, 2012.

Sanchez, J., Tanner, D., Chen, D., Huey, L., and Ng, N.: A new technique for the direct detection of HO₂ radicals using bromide chemical ionization mass spectrometry (Br-CIMS): initial characterization, ATMOSPHERIC MEASUREMENT TECHNIQUES, 9, 3851-3861, 10.5194/amt-9-3851-2016, 2016.
Shaw, M. and Carpenter, L.: Modification of Ozone Deposition and I2 Emissions at the Air-Aqueous Interface by Dissolved Organic Carbon of Marine Origin, ENVIRONMENTAL SCIENCE & TECHNOLOGY, 47, 10947-10954, 10.1021/es4011459, 2013.
Sherwen, T., Evans, M. J., Carpenter, L. J., Andrews, S. J., Lidster, R. T., Dix, B., Koenig, T. K., Sinreich, R., Ortega, I., Volkamer, R., Saiz-Lopez, A., Prados-Roman, C., Mahajan, A. S., and Ordonez, C.: Iodine's impact on tropospheric oxidants: a global model study in GEOS-Chem, Atmospheric Chemistry and Physics, 16, 1161-1186, 10.5194/acp-16-1161-2016, 2016a.
Sherwen, T., Schmidt, J., Evans, M., Carpenter, L., Grossmann, K., Eastham, S., Jacob, D., Dix, B., Koenig, T., Sinreich, R., Ortega, I., Volkamer, R., Saiz-Lopez, A., Prados-Roman, C., Mahajan, A., and Ordóñez, C.: Global impacts of tropospheric halogens (Cl, Br, I) on oxidants and composition in GEOS-Chem, ATMOSPHERIC CHEMISTRY AND PHYSICS, 16, 12239-12271, 10.5194/acp-16-12239-2016, 2016b.
Simpson, W. R., Brown, S. S., Saiz-Lopez, A., Thornton, J. A., and von Glasow, R.: Tropospheric Halogen Chemistry: Sources, Cycling, and Impacts, Chemical Reviews, 115, 4035-4062, 10.1021/cr5006638, 2015.
Sipilä, M., Sarnela, N., Jokinen, T., Henschel, H., Junninen, H., Kontkanen, J., Richters, S., Kangasluoma, J., Franchin, A., Peräkylä, O., Rissanen, M., Ehn, M., Vehkamäki, H., Kurten, T., Berndt, T., Petäjä, T., Worsnop, D., Ceburnis, D., Kerminen, V., ..., and O'Dowd, C.: Molecular-scale evidence of aerosol particle formation via sequential addition of HIO₃, NATURE, 537, 532-534, 10.1038/nature19314, 2016.
Sjostedt, S. and Abbatt, J.: Release of gas-phase halogens from sodium halide substrates: heterogeneous oxidation of frozen solutions and desiccated salts by hydroxyl radicals, ENVIRONMENTAL RESEARCH LETTERS, 3, 10.1088/1748-9326/3/4/045007, 2008.
SOLOMON, S., GARCIA, R., and RAVISHANKARA, A.: ON THE ROLE OF IODINE IN OZONE DEPLETION, JOURNAL OF GEOPHYSICAL RESEARCH-ATMOSPHERES, 99, 20491-20499, 1994.
Stark, H., Yatavelli, R., Thompson, S., Kimmel, J., Cubison, M., Chhabra, P., Canagaratna, M., Jayne, J., Worsnop, D., and Jimenez, J.: Methods to extract molecular and bulk chemical information from series of complex mass spectra with limited mass resolution, INTERNATIONAL JOURNAL OF MASS SPECTROMETRY, 389, 26-38, 10.1016/j.ijms.2015.08.011, 2015.
Tham, Y. J., He, X. C., Li, Q. Y., Cuevas, C. A., Shen, J. L., Kalliokoski, J., Yan, C., Iyer, S., Lehmusjarvi, T., Jang, S. H., Thakur, R. C., Beck, L., Kemppainen, D., Olin, M., Sarnela, N., Mikkila, J., Hakala, J., Marbouti, M., Yao, L., ..., and Sipila, M.: Direct field evidence of autocatalytic iodine release from atmospheric aerosol, Proceedings of the National Academy of Sciences of the United States of America, 118, 8, 10.1073/pnas.2009951118, 2021.
Vogt, R., Sander, R., Von Glasow, R., and Crutzen, P.: Iodine chemistry and its role in halogen activation and ozone loss in the marine boundary layer: A model study, JOURNAL OF ATMOSPHERIC CHEMISTRY, 32, 375-395, 10.1023/A:1006179901037, 1999.
Wang, M., Kong, W., Marten, R., He, X., Chen, D., Pfeifer, J., Heitto, A., Kontkanen, J., Dada, L., Kurten, A., Yli-Juuti, T., Manninen, H., Amanatidis, S., Amorim, A., Baalbaki, R., Baccarini, A., Bell, D., Bertozzi, B., Bräkling, S., ..., and Donahue, N.: Rapid growth of new atmospheric particles by nitric acid and ammonia condensation, NATURE, 581, 184-+, 10.1038/s41586-020-2270-4, 2020.
Wang, M. Y., He, X. C., Finkenzeller, H., Iyer, S., Chen, D. X., Shen, J. L., Simon, M., Hofbauer, V., Kirkby, J., Curtius, J., Maier, N., Kurtén, T., Worsnop, D. R., Kulmala, M., Rissanen, M., Volkamer, R., Tham, Y. J., Donahue, N. M., and Sipilä, M.: Measurement of iodine species and sulfuric acid using bromide chemical ionization mass spectrometers, Atmospheric Measurement Techniques, 14, 4187-4202, 10.5194/amt-14-4187-2021, 2021a.
Wang, X., Jacob, D., Downs, W., Zhai, S., Zhu, L., Shah, V., Holmes, C., Sherwen, T., Alexander, B., Evans, M., Eastham, S., Neuman, J., Veres, P., Koenig, T., Volkamer, R., Huey, L., Bannan, T., Percival, C., Lee, B., and Thornton, J.: Global tropospheric halogen (Cl, Br, I) chemistry and its impact on oxidants, ATMOSPHERIC CHEMISTRY AND PHYSICS, 21, 13973-13996, 10.5194/acp-21-13973-2021, 2021b.
Yeoman, A., Heeley-Hill, A., Shaw, M., Andrews, S., and Lewis, A.: Inhalation of VOCs from facial moisturizers and the influence of dose proximity, INDOOR AIR, 32, 10.1111/ina.12948, 2022.

Zhang, Y., Liu, R., Yang, D., Guo, Y., Li, M., and Hou, K.: Chemical ionization mass spectrometry: Developments and applications for on-line characterization of atmospheric aerosols and trace gases, TRAC-TRENDS IN ANALYTICAL CHEMISTRY, 168, 10.1016/j.trac.2023.117353, 2023.